Vacuum Vessel and Limiter for ZEPHYR

H. Kotzlowski, H.-J. Kutsch
K.F. Mast, H. Vernickel

IPP 1/202 April 1982

Reprint of ZEPHYR-Report No. 19 of July 1980.

MAX-PLANCK-INSTITUT FÜR PLASMAPHYSIK

8046 GARCHING BEI MÜNCHEN

MAX-PLANCK-INSTITUT FÜR PLASMAPHYSIK

GARCHING BEI MÜNCHEN

Vacuum Vessel and Limiter for ZEPHYR

H. Kotzlowski, H.-J. Kutsch
K.F. Mast, H. Vernickel

IPP 1/202 April 1982

Reprint of ZEPHYR-Report No. 19 of July 1980.

Die nachstehende Arbeit wurde im Rahmen des Vertrages zwischen dem Max-Planck-Institut für Plasmaphysik und der Europäischen Atomgemeinschaft über die Zusammenarbeit auf dem Gebiete der Plasmaphysik durchgeführt.

Vacuum Vessel and Limiter for ZEPHYR

H.Kotzlowski, H.-J.Kutsch, K.F.Mast, H.Vernickel
Max-Planck-Institut für Plasmaphysik, EURATOM-Association,
D-8046 Garching, Germany

Abstract

This report describes the design of the vacuum vessel and of the limiter for ZEPHYR. The vacuum vessel is a welded structure consisting of rigid sectors and bellows. The limiter is a large area toroidal limiter completely covering the inner side of the torus wall. It is subdivided into many small elements in order to allow for free thermal expansion and to reduce eddy current forces. Stress analysis of the vessel is presented as are considerations for plasma-surface interaction and for remote repair of vessel and limiter.

Vacuum Vessel and Limiter for ZEPHYR

1. Introduction

In this report we describe the vacuum vessel and limiter of ZEPHYR. Most of the work is a continuation of a development as described in the Status Report of September 78 /1/ and IPP Report 1/175 /2/.

Early optimization studies demonstrated that the distance between the plasma and TF coils governs the total outlay. The small value of 9 cm between the plasma boundary and coil at the throat was therefore chosen as a design goal.
The most severe load which the vessel has to withstand is the forces during a hard plasma disruption. These forces were the basis for the stress analysis of the present design /2/. The basic features of the design can be summarized as follows:
The vessel will be an all metal structure without insulating breaks. It consists of 16 wedge-shaped shell sectors of a box profile connected by double-walled, parallel bellows. Within the magnet and cool box all components of and connections to the vessel are joined by full penetration welds (instead of elastomers or metal sealed connections). The necessary electrical resistance is brought about by the corrugated bellows, while the shell segments provide access to the interior for assembly, testing, pumping, neutral injection and diagnostics.
Mechanically the vessel has to be supported by the magnet since no space for a self-supporting structure is available.

The material for the vessel structure is Inconel 625. This alloy was chosen for its high mechanical strength and large resistivity.
On the inside the surface is protected by a thermal shield combined with a large area limiter /3/. The limiter consists of individual mushroom-like elements which are mounted with bayonet catches on Inconel plates. The mushrooms consist of graphite, covered with a thin layer of TiC.

Chapter 2 of this report presents the arguments for the actual design, a more detailed description of it and calculations to determine the forces on the vessel and the resulting

stresses and strains. Chapter 3 describes the limiter and heat shield, chapter 4 and 5 indicate present ideas on cleaning, limiter sputtering and remote handling. The figures used in this report stem from various stages of the design, hence the slight variation in parameters that may be noted in the captions.

2. Vacuum Vessel

2.1 Requirements and Boundary Conditions

The vacuum vessel of ZEPHYR has to provide an environment in which the plasma can be produced, heated, compressed, ignited, and diagnosed. These requirements have to be fulfilled under critical boundary conditions not yet found together in any other comparable experiment:

- Situated inside the cool box of the magnet, the vacuum vessel will be operated at a temperature between 300 K and 80 K (possibly 40 K).
- Because of the high thermal loads coming from the plasma losses (up to 3 MW/m^2 for 5 s at the throat) and ripple losses of neutral injection (up to 5 MW/m^2 for 1.5 s at certain locations) part of the inner surface of the vessel has to be protected by a heat shield.
- High electrical resistance of any part the vessel structure is required, especially equally distributed electrical resistance around the toroidal path formed by the vessel wall.
- Magnetic permeability has to be < 1.01.
- For neutral injection 6 horizontal ports 380 mm in width and 780 mm in height at $\alpha = 20^\circ$ have to be provided [1].
- Diagnostic ports and pumping ports are necessary.
- The vessel may require a separate cooling system (260 MJ will be deposited as thermal energy in the vessel structure during a full power discharge, the repetition rate being up to 60 min).
- Already after few DT-discharges the vessel structure will be fully activated and has therefore to be capable of remote maintenance and repair.
- The requirement for a minimum magnetic volume of the magnet and the compression of 1.5 lead to a compact arrangement of the tokamak system with a distance plasma/TF coil of 9 cm and a noncircular shape of the vessel.
- During a hard plasma disruption the vessel shell will be locally stressed with up to 80 x atmospheric pressure.

(1) 4 to 6 ports; beam width is 300 mm, beam height 720 mm, beam angle at center of port (at 3020 mm) is 14 - 26°.

- The outgassing rate for all gases except hydrogen has to be below 10^{-9} mbar l/s cm^2 (it may be one order of magnitude larger for hydrogen).
- The leak rate has to be $< 10^{-6}$ mbar · l/s.

Some data of the vessel are collected in Table I. Information on the number of load cycles is contained in the Internal ZEPHYR Report 21 /17/.

2.2 Concept Studies

The vacuum vessel can be designed with thick walls and without bellows as a uniform wall shell, a ring/ribs-stiffened shell, a bellows structure or any combination of the above as a self-supporting or externally supported structure. By relying on external support, the strength margins against collapse can be traded off if necessary to satisfy other requirements. In ZEPHYR there are electromagnetic considerations in addition to space limitations which drive the structural design in this direction. As already listed, these requirements are

- relatively high electrical resistance of any part of the structure to minimize stray fields and the electromagnetic forces on the structure caused by eddy currents.
- sufficiently high and equally distributed electrical resistance around the toroidal path, formed by the vacuum vessel wall, in order to minimize vertical stray fields, which may delay or even prevent breakdown of the gas. (The minimum value necessary for the toroidal resistance has to be investigated in detail, but a sharp limit is not to be expected. For the time being 1 m , which is approximately twice the resistance of the plasma at 5 eV, was used as a guidline.

Satisfactorily high electrical resistance of the vessel shell can be obtained in several ways:

- The vessel could be constructed from high-resistivity materials
- The effective cross-sectional area of the vessel wall could be reduced by using thin shell structures with local stiffeners or a sandwich design
- Ceramic insulators could be built into the shell wall at two or more locations
- The toroidal length of the shell could be increased by using membrane or corrugated bellows. (The last two possibilities modify the resistance in the toroidal direction only.)

However, each of these approaches has limitations :

The resistivity of all available metallic construction materials is too low for the first solution. Fabriaction of the vessel from glass or ceramics is not considered because of their low ductility and high sensitivity to temperature gradients, joining problems etc.

Reducing the cross-sectional area of the vessel wall by using thin shells with local stiffeners or a sandwich structure is limited owing to the difficulty of attaching large ports, heat shields or assembly flanges. Without being externally supported such a vessel would not withstand the electromagnetic forces during a hard plasma disruption. But external supports hinder thermal movements of the vessel and thus again generate stresses in the shell.

The desired toroidal electrical resistance can be obtained by ceramic insulators built into the toroidal wall at two or more locations. This concept, if designed to be self-supporting, gives the maximum independence with respect to the magnet in terms of development, manufacture, testing and assembly. Its approx. 2 cm thick shell requires a minimum of space between the plasma and magnet. For assembly purposes the vessel has to be split into two oppositely situated vertical planes, or eight in the case of a modular concept of the device. Ceramic or glass insulators for this application are not currently available and there is little confidence in getting a sufficiently reliable solution developed in time. More promising seem to be thin ceramic coatings such as plasma-sprayed multi-layers of pure alumina and a mixture of Al_2O_3 and $Ti\ O_2$ with a total thickness of 0.3 - 0.6 mm, as successfully applied in TF /4/.

However designed, the electrical break will always be more sensitive to large stresses and deformations than the undisturbed vessel shell. As the results of a detailed investigation show /2/ the maximum stressing of the vessel occurs at the electrical discontinuities of the shell. During the compression phase of the plasma antiparallel line currents of equal magnitude flow along each electrical break in the shell. On interacting with the toroidal field they produce electromagnetic shear forces of max. 1800 N/mm, which have to be transmitted via the electrical insulation. Finitely distributed (toroidal direction), these forces additionally twist the connection flanges and generate stresses of 800 MPa in the insulation. As all efforts to reduce these stresses require more space between the plasma and coils (approx. 20 cm), this type of vessel has not been further investigated.

Another possibility of obtaining the desired toroidal electrical resistance of the vessel is the use of membrane bellows. However, the low inherent reliability associated with the several kilometers of welds necessary to fabricate the bellows is undesirable and must be compensated for by an extensive and expensive quality assurance effort. Corrugated bellows, formed hydraulically or by rolling, reduce the welds by a factor of 10 and, unfortunately, the resistance by a factor of 2.5

2.3 Design of the Vacuum Vessel

Among the investigated concepts, the complete welded structure composed of bellows and shell segments, fabricated from the high-nickel alloy INCONEL 625, seems to fulfill best the requirements for the vacuum vessel of ZEPHYR. Most of the large tokamaks are equipped with vessels of this type. But their designs differ considerably (see Table II), because each one has to provide an interface compatible with a different, device-specific tokamak system.

In ZEPHYR the most severe restriction for the vessel design is imposed by the TF magnet. Its concept, geometry, number of coils, design of the supporting structure, access to the vessel , separation method of the device and cooling concept, as well as the requirement for thermal shielding of the inner surface of the vessel form the design basis for the vacuum vessel. As these boundary conditions are still under investigation, the development of the vessel concentrated on principal design solutions.

Situated inside the magnet, the vessel has the noncircular shape of the coils (Fig. 1). Along its poloidal circumference the thickness of the wall varies from 50 mm (throat) to 115 mm (support) and 85 mm (NI port), while the thickness of the thermal shield combined with the large-area limiters is 40 mm. Toroidally the vessel wall is subdivided into 16 parallel bellow sections and an equal number of wedge-shaped shell segments (Fig. 2).

The bellows, necessary for a higher toroidal electrical resistance of the vessel, destroy the stiffening effect of a continuous toroidal shell. Without any external radial support such a structure would already collapse at atmospheric pressure, since no space for mechanical bridging of the bellows is available. Calculations have shown that an additional vertical support will reduce the stresses in the shell by a factor of 2.5 (Fig. 3). In order to withstand the antimetric (tilting) forces during a plasma disruption these supports have to be placed along the edges of the shell segments. Otherwise large deformations of the shell segments of $\pm$ 18 mm (still elastic) would lead to overstressing of the bellows. Additional supports in the midplane serve to position the vessel and limit its movements (Fig. 4). It is obvious that such integration of the vessel into the magnet (16 x 14 = 224 supports) re-

quires a suitable magnet concept.

The bellows sections can be designed as single or double-walled by using corrugated bellows. A single-wall structure (Fig. 5a) yields 0.8 mΩ, which is almost the desired toroidal electrical resistance of the vessel, but also entails 400 metres of 2 mm thick vacuum welds which are difficult to leak test during manufacture and assembly, especially at low temperatures. Besides, the bellows are the most stressed part of the vessel and inaccessible for repair. A second wall, as shown in Fig 5b would be a safeguard in case the inner bellow should fail or develop a leak. However, this would be at the expense of lower resistance (0.4 mΩ) anda more complicated and expensive construction of the vessel. The lower resistance reduces the tilting forces during disruption by a factor of 2, the presence of two walls halves the load per bellow (except for atmospheric pressure). During operation the interspace between the bellows could be pumped by a separate vacuum system to a pressure of around 10^{-3} torr. This double bellow concept is therefore favoured for the vessel design.

Mechanically, the bellows have to fulfill two contradictory requirements. On the one hand they have to absorb elastically relative movements of the shell segments, which calls for high elasticity. On the other hand they have to sustain loads which require a stiffness similar to those of the shell segments. Any compromise leads to extremely high stresses in the bellows and necessitates

- avoidance of stress concentration in the bellows and in the welds to the shell segments
- full-penetration welds using filler metal
- stress relieving after welding
- limitation of the deflection of the inner bellow by the thermal shields
- reduction of stresses at the outer bellows by increasing the curvature in the flat region (see Fig. 7).

The subdivision of the vessel into 16 bellows / shell units seems to be optimal for the present parameters of ZEPHYR. Smaller subdivision would give a lower electrical resistance and larger tilting moments. A larger one would increase the number of welds, supports and heat shields, while the width of the NI ports is reduced. A different aspect ratio and/or compression

ratio would change this situation.

The shell segments incorporate all penetrations through the vessel wall. The largest one, the NI duct, is an integral part of the structure. Smaller ports for diagnostics have to be welded on after assembly and from inside the vessel. Along the edges of the shell segments the heat shields, carrying elements of the large-area limiter, are welded on by circular welds 25 mm in diameter (see Fig. 15). In order to obtain high stiffness the shell segments have a box-shaped profile. The interspace can be used for gas flow is separate cooling of the vessel or a more uniform temperature distribution after a discharge is necessary. Its access from outside is incorporated into the NI port as well as that to the bellows-interspace.

The assembly of the vessel has to be done jointly with the magnet, since one coil together with a shell segment and bellows section forms a unit. At the weld the vessel will be single walled. However, it will be placed in a low-stress region, be 8-10 mm thick and possibly use electron beam technique. The assembly process is illustrated in Fig. 6.

A modification of this type of vessel is complete integration of the shell segments into the mechanical structure of the magnet. Such a concept would give the maximum possible compact arrangement of the device (Fig. 8). In the next step of the design phase this proposal will be investigated in more detail as a back-up solution.

2.4 Stress Analysis

2.4.1 Electromagnetic Forces in the Vacuum Vessel

During operation of ZEPHYR, time-varying magnetic fields will induce eddy currents in the wall of the vacuum vessel due to the finite resistivity of the wall material. Two main effects can be ascribed to them: generation of magnetic stray fields in the plasma and production of electromagnetic forces on the vessel. The stray fields are primarily of importance during the start-up phase.* The OH transformer mainly induces toroidal eddy currents, whose stray fields render start-up more difficult /5/. In the following we are concerned with the forces on the vessel. They are caused by the interaction with the toroidal and poloidal fields. Only the principal electromagnetic loads which will influence the vessel design together with their excitation mechanisms are described.

The eddy currents on the vacuum vessel are calculated on the assumption that the vessel can be represented as a thin shell, e.g. no current flows in the direction normal to the vessel surface. This assumption is justified since any radius of curvature of the vessel is much larger than the wall thickness and the magnetic energy stored in the fine structure of the vessel wall is negligible compared with the whole magnetic energy of the vessel. The thin shell was set in the centre of the vessel wall.

The eddy current disbribution derived with this thin-shell approximation describes with sufficient accuracy the magnetic stray fields in the plasma region as well as the total electromagnetic loads on the bellows or shell sectors and the vessel supports. By running these eddy currents over the real fine structure of the vessel the exact load distribution on the different vessel parts can be calculated to yield the input for the FE stress analysis.

Since the corrugation increases the path length in the toroidal direction, but the cross-section in the poloidal direction, an anisotropic surface resistivity was introduced in order to describe correctly the difference in toroidal and poloidal resistivity. In the case of double-walled vessel segments the calculated electromagnetic loads will be divided into equal parts, each wall being loaded in the same manner.

---

* During compression the stray fields from the main field coils dominate the disturbance of the plasma (see report on TF coils /14/).

On a conducting thin shell any eddy current distribution can be represented by a series of orthogonal eigenmodes which are energetically decoupled and are given by

(1) $$\vec{j}_n(\varrho, t) = \vec{j}_n(\varrho) \cdot e^{\lambda_n \cdot t} \qquad \lambda_n < 0 \text{ , real}$$

The most critical electromagnetic loads on the vessel, far exceeding atmospheric pressure, are induced by hard disruption of the plasma current in the compressed state. Critical loads will also occur during the rise or decay of the toroidal magnetic field, especially if the TF magnet is rapidly switched off under fault conditions.
In both cases the eigenmodes with small eigenvalues have to be considered in determining the eddy current distribution /2/. For the calculation wedge-shaped bellows have been assumed, such that the interfaces between bellows and shells are on planes φ = const in a toroidal system of coordinates. The characteristic features of these modes are as follows:

1. Eigenmode of pure poloidal currents which only interacts with the toroidal magnetic field, yielding loads normal to the vessel surface. The mode is featured by the smallest eigenvalue of all and will be excited by time-varying toroidal magnetic fields and diamagnetic plasma current.

2. Eigenmode of pure toroidal currents which interact with the vertical magnetic field and mutually. The loads are axisymmetric and have components normal and tangential to the vessel surface. This mode is excited by changes in vertical field and by changes in plasma current. It is accompanied by eigenmode 3.

3. Eigenmode of toroidal dipole current coupled with closed saddle currents flowing on each shell and bellows sector caused by periodic toroidal discontinuities of the surface resistivity at the bellows-shell interface (Fig. 9). On an axisymmetric vessel the saddle currents would disappear. The toroidal current interacts with the vertical magnetic field and mutually while the saddle currents mainly interact with the toroidal magnetic field yielding tilting forces on the shell segments.

Although the loads during rise and decay of the toroidal magnetic field are not as severe as those during disruption, they unavoidably occur at every shot and are the major load in the absence of disruption. They are described first:

During the rise or decay of the toroidal magnetic field the eigenmode 1 will be excited causing electromagnetic pressure loads on the vessel. The maximum loads will occur at the end of the rise or decay of the toroidal field and their mean value averaged in the toroidal direction is described by

$$(2) \qquad \langle p_M \rangle_{TF} = \frac{1}{\mu_0} \cdot B_T^2(R) \, \frac{\tau_\sigma}{\tau_r} \left(1 - e^{-\tau_r/\tau_\sigma}\right)$$

τ_r = rise- or decay time of the toroidal field

$\tau_\sigma = 1/\lambda_1$ = time constant of the poloidal eigenmode 1

$B_T(R)$ = toroidal field

R = major radius

The pressure loads on the bellows and shell sectors are obtained by multiplying $\langle p_M \rangle_{TF}$ by appropriate geometry factors. They are given in the appendix together with the derivation of equations (2) and (3).

During a disruption of the plasma current the mode 1 will be excited by diamagnetic plasma currents. By assuming an exponential decay of the plasma current during disruption the maximum toroidally averaged load is given by

$$(3) \quad \langle p_M \rangle_D = \frac{1}{\mu_0} \cdot \frac{|\tilde{\Phi}_T|}{\Phi_{TV}} \cdot \frac{B_T^2(R)}{\left(\frac{\tau_\rho}{\tilde{\tau}_G} - 1\right)} \left[e^{-t_0/\tau_\rho} - e^{-t_0/\tilde{\tau}_G} \right]$$

with

$$(4) \quad t_0 = \ln\left(\frac{\tilde{\tau}_G}{\tau_\rho}\right) \Big/ \left[\frac{1}{\tau_\rho} - \frac{1}{\tilde{\tau}_G}\right]$$

τ_ρ = decay time of plasma current

Φ_{TV} = total toroidal magnetic flux in the vessel without plasma

$\tilde{\Phi}_T$ = diagmagnetic flux.

The diamagnetic flux was derived from a cylindrical model /2/ ($A \to \infty$) as

$$(5) \quad \tilde{\Phi}_T = \frac{\mu_0^2}{8\pi} \cdot \frac{1-\beta_\rho}{\langle B_T \rangle} \cdot I_{\rho L}^2$$

If $\tau_\rho \ll \tau_\sigma$ the pressure on the vessel is equal to the average pressure $\langle p_M \rangle_D$, while in the case $\tau_\rho \geq \tau_\sigma$ the geometry factors of the appendix again have to be applied.

During a hard plasma disruption the main loads are caused by eigenmodes 2 and 3, which have already been described in /2/. Since eigenmodes 2 and 3 are strongly coupled ohmically by the cylindrical bellows of the vessel, their excitation must be treated together. It was shown in /2/ that the saddle currents are much smaller than the toroidal currents in the case of the vessel geometry of ZEPHYR. It is therefore possible to derive the toroidal current components of modes 2 and 3 independently of the saddle currents by dividing the vacuum vessel into 40 toroidal conductors with the correct resistance and inductively coupling them, with the plasma and mutually. One gets the surface current density of the toroidal eddy currents by averaging the conductor currents in the poloidal direction.

The poloidal current density $j^{(v)}$ of the saddle currents on the shell and bellow sectors is mainly determined by the poloidal gradient of i_φ . The tilting pressure distribution on the shell and bellows sectors arises from the interaction of $j^{(v)}$ with the toroidal field with its maximum value at the interfaces between the shell and bellows sectors. Detailed information about the electromagnetic loadings caused by mode 2 and 3 are given in /2/. The toroidal eddy currents interact mutually and with the vertical magnetic field resulting in axisymmetric forces. In Fig. 10 the poloidal distribution of the maximum tilting pressures along the interface between the bellows and shell sectors is represented for hard plasma disruption. As a result the importance of the diamagnetic loads with regard to the total axisymmetric loads increase with increasing current decay time due to the larger time constant of the poloidal mode.

The determination of the electromagnetic forces during disruption needs further refinement in the future. Calculations with a more detailed finite element code are envisaged as well as measurements on an electrical model. The scaling laws and the measuring procedure to be applied are described in /6/.

2.4.2 Stress Analysis

During a discharge the vessel structure undergoes a steadily altering combination of thermal, electromagnetic and mechanical loads. The use of materials with different thermal expansion, nonuniform temperature distribution and movements of the supports additionally prestresses the vessel. The starting temperature will not be the same for all discharges, since at low temperature difference, the cooling time of 30 min is not sufficient to remove all of the energy dissipated by the structure. In view of the complicated and design-specific loads, the stress analysis concentrated on the detection of critical loads. The rough optimization of the design with respect to the stresses was made with a max. permissible value of 300 MPa (yield strength of Inconel 625 ($\sigma_{0,2}$) is 420 MPa). The critical loads are:

- Prestress due to temperature difference to the magnet. For instance if ΔT = 200 K (i.e. magnet at 80 K and vessel at 280 K) the calculated stresses are shown in Fig. 11 with a maximum value of 150 MPa. Higher temperature differences give proportionally higher stress.

- Nonuniform heating of the wall normal to and along the shell is expected to be in the range of 150 K. Depending on the distribution this will lead to additional stresses of approx. 100 MPa.
  In the next step of the design optimization this problem will be investigated in more detail, together with the cooling of the vessel.

- Thermal loading of the inner wall surface requires introduction of a heat shield as mentioned in section 2.1. In order to prevent short circuiting of the bellows, arcing and to allow movements, the tiles of the shield have to be arranged with gaps in between of up to 15 mm. The effect of the shine-through of the plasma to the bellows has still to be investigated.

- Thermal and elastic movements of the magnet are not known up to now, but they are expected to be in a tolerable range.

- Reaction forces coming from the NI ducts, pumping and diagnostic ports are still to be investigated.

- Electromagnetic forces during the rise/drop of the toroidal field. The stresses for this load case are given in Fig. 3. They are smaller than those during disruption.

- Electromagnetic forces during a plasma disruption. These forces produce the greatest mechanical stress of the vessel, thus governing its reliability and life time. As their intensity, distribution and time development strongly depend on the vessel design, the calculations and optimization of the vessel design have to be accomplished in steps. The results of the last analysis are shown in Figs. 12, 13. The most stressed parts of the vessel are the bellows, where the stresses reach values of 500 MPa. This requires the already mentioned limitation of the deflection of the inner bellows, a larger curvature of the outer bellows and some of the supports of Fig. 4. With these changes in the design, the stresses will probably be reduced to approx. 300 MPa. For more detailed information see /2/.

Table III gives the reaction forces, calculated for each load case, which have to be transmitted by the radial supports. Owing to the lack of space and the large forces (up to 200 kN) no electrical insulation can be built into the supports. In order to prevent short-circuiting of the bellows, electrical breaks of the magnet have to be placed between the supports. (These breaks also prevent a toroidal short-circuit via the magnet casings).

The linear, static analysis of the vessel was done using the finite element program STRUDL II. Fig. 14 shows the calculation model consisting of 614 shell elements.

3. Limiter and Heat Shield

3.1 Design

The heat shield on the inside of the torus (at the "throat") and in addition the shield of the bellows will serve as limiter. This then is a toroidal limiter at the throat, which will extend to about 45° above and below the equatorial plane (total surface area about 7 m^2) and 16 poloidal limiters of width 0.2 m which the uncompressed plasma should touch on a total area of about 6 m^2.

The limiter proper consists of individual mushroom-like elements (see Fig. 15), which may be manufactured from various materials. At present we consider them to be graphite (a low-Z material resistant to thermal shock) which will be coated with e.g. TiC in order to supress CH_4 formation. Coatings that withstand the load under normal operating conditions are described in the literature, e.g. /7, 8/. These elements are mounted with bayonet catches on Inconel plates which in turn are welded to the shell sectors. The space factor with this construction is about 0.5, the true limiter surface therefore is about 3 m^2 before and after compression. This design allows free thermal expansion of the limiter elements and also reduces eddy currents owing to the small size. Since the limiter surface is nearly parallel to the magnetic field, the plasma will penetrate only a small distance between the individual mushrooms. The mounting plates therefore experience only radiation and charge exchange neutrals.

3.2 Thermal Load on the Limiter and Resulting Temperatures

3.2.1 Normal operating conditions

The average power flux through the plasma surface is about 0.4 and 0.7 MW/m^2 before and after compression. Radiation and charge exchange loss leave the plasma more or less homogeneous, while transport losses are concentrated on the limiter. Although (see below) a large part of the energy loss will be radiated, a certain, possibly local, concentration of the heat load on the limiter cannot be excluded. We therefore require the limiter to withstand regularly a load of 3 MW/m^2 during 5 s. The temperature rise per MW/m^2 calculated for plane geometry and with constant coefficients / 9 /, is presented in Fig.16. While the Inconel surface would become too hot, the graphite surface easily stays within permissible limits.

In the 30 to 60 min intervals between shots the limiter will cool down by radiation alone to 500 - 600° K in "steady state", i.e. if a shot is fired every 30 or 60 min (Fig. 17), this being again a permissible temperature.

The bayonet catches fixing the mushrooms may not be heated beyond 400° C. Preliminary tests have been made in the following way:
A limiter element was placed in a "mounting plate", and the temperature was measured at various positions (Fig. 18). The limiter front was heated in argon by electromagnetic induction until the front reached 1000° C. The heating power was then switched off. As an example we present the results of a run in which the mushroom was pressed into a SS plate with varying forces (Fig. 19). Cooling under these conditions is sufficient to keep the mounting spring to temperatures below 500° C even with this long heating time. More detailed measurements with the set-up in vacuum to determine the coefficient of heat transfer between mushroom and mounting plate are in preparation.

3.2.2 Plasma disruption

The energy content of the compressed plasma is 20 MJ, of which 14 MJ is kinetic energy of the plasma particles, the rest being magnetic energy of the poloidal field inside the plasma column. If this energy is uniformly emitted in all directions, a load of 0.75 MJ/m^2 is deposited at the throat (or 750 MW/m^2 in the case of a 1 ms disruption). For graphite this would result in the evaporation of less than one monolayer / 10 /. If energy deposition is, however, not uniform, local damage cannot be excluded.

3.3 Electromagnetic Forces on the Limiter Supporting Plates

The most critical electromagnetic loads on the limiter supporting plates will be caused by hard plasma disruption. Since the transverse dimensions of the supporting plates of the limiter mushrooms are much larger than the plate thickness, only the magnetic field component normal to the plate surface has to be considered for calculating the eddy currents in the plates. Because of the close mounting of the supporting plates parallel to the vessel surface the magnetic field component normal to a supporting plate can be set equal to that normal to the vessel surface. The maximum electromagnetic forces will be induced by plasma disruptions with current decay times shorter than the toroidal time constant of the vacuum vessel. In this case (considered exclusively in the following) the eddy currents in the supporting plates

are excited by the magnetic field of the eddy currents on the vacuum vessel decaying with the toroidal time constant of the vessel.

When the plasma current has just disappeared the initial magnetic field of the eddy currents on the vessel is the same as the poloidal magnetic equilibrium field of the plasma. A linear ramp function was therefore assumed for the decay of the normal component of the magnetic field.

The eddy currents flowing perpendicularly to the toroidal magnetic field interact with it and cause large bending moments on the welding seams connecting the supporting plates with the shell sectors.

Fig.20 represents the electromagnetic forces per unit length on the supporting plates as a function of the poloidal circumference of the vacuum vessel. The forces for plasma disruptions in the compressed and uncompressed states are shown. Fig. 21 compares the electromagnetic forces per unit length for supporting plates of different composition. Plates of Cu-Inconel 625 compound material feature the advantage of high thermal conductivity but suffer high electromagnetic loads especially at LN_2 temperature. The bending stresses of 200 MPa caused in the latter case at the welding seams are fairly large. Since radiation cooling of the limiter seems possible, as mentioned above, the option of a high thermal conductivity mounting plate will not be pursued at the moment.

4. Plasma Surface Interaction

4.1 Cleaning

Apart from the usual chemical cleaning before assembly the final in-situ cleaning will be done by glow discharge cleaning (GDC) and by low-power discharge cleaning (LPDC). These are well established cleaning methods (see, for example, Dylla /12/).

With the proper choice of parameters GDC penetrates into recessed areas and it will thus also be possible to clean the spaces behind the limiter mushrooms. Discharge cleaning will be performed with H or D but not with T in order to avoid implantation of T into the bellows and the handling of large amounts of tritium.

Lower power discharges in D, T, but with pulsed gas influx and therefore reduced gas throughput will be used as conditioning discharges in order to produce the proper composition of the recycling gas in the wall. The optimum sequence of cleaning and conditioning discharges for the case that cleaning between shots proves necessary, has not yet been discussed in any detail.

Simulation tests of the cleaning methods are planned in order to determine optimal parameters for cleaning the recessed areas.

In-situ gettering is not suggested at present. If necessary, getter panels can be attached at the upper or lower parts of the shell sections. Details have not yet been worked out.

The effectiveness of cleaning determines, in particular, the low-Z impurities (O, C) during the build-up phase of the plasma and therefore the heating energy required during plasma build-up.

Since a large part of the inner surfaces may be cooled to about LN_2 temperatures in between shots, since gaseous molecules such as CO, CO_2, CH_4, H_2O etc. are easily adsorbed at these temperatures but are also easily desorbed by interaction with the plasma, any such impurity left over from the previous shot or introduced during the interval from NI, diagnostics, leaks etc. is a potential source of low-Z impurities.

$Z_{eff} = 2$ corresponds to about 5×10^{19} oxygen or carbon atoms in the plasma (corresponding to a desorption of $\sim$ 1/10 of a monolayer of the geometrical inner surface of the vessel). This amount could accumulate during 30 min if the total leak rate were $\sim 10^{-3}$ mbar · l/s. Cleaning discharges before every shot certainly cannot be avoided if the leak rate is of that order or larger.

4.2 Erosion

Sputtering by charge exchange neutrals will occur on the entire wall, and erosion by arcing and sputtering due to ions primarily on the limiter. If the plasma sheath is collision dominated, the sheath potential in the ZEPHYR geometry will be small ($\ll kT$), as discussed in /3/.* In this case arcing should be absent. Ion sputtering which is coupled to the transport loss has also been discussed in /3/. The resulting sputtering rate for a transport loss of 8 MW as a function of the boundary temperature (which is considered a free parameter) is presented in Fig. 22. This impurity influx will increase the radiation loss and therefore decrease transport loss. Related physics questions such as the existence of a "photosphere" are discussed in a companion report /15/. The important conclusion for the limiter is that no large transport loss is expected at the limiter during the steady burn phase.

---

* If the sheath is collisionless, the sheath voltage will be around 4 kT as in the case of the "normal" geometry, where the magnetic field intersects the limiter at right angles /11/. This would change details in the calculation of the erosion rate, but does not change the order of magnitude.

5. Remote Handling

According to the remote handling concept of ZEPHYR the vessel has been designed for modular assembly and disassembly in the event of failure in the magnet or vessel.
The size of the replaceable units can be adapted to the extent of the failure. Its upper limit is given by the capacity of the crane (probably 10^6 N) as the shell segments are rigidly connected with the coils.
For disassembly two bellows sections have to be cut apart using electron beam technique or laser cutting or by milling and grinding. The remaining parts of the destroyed bellows then have to be removed by milling. The new vessel unit always consists of one bellows section more than shell segments and will be welded on after the magnet is closed. The complete procedure is as follows:

1. opening at one or more NI ports
2. removal of the respective limiters (automatic device)
3. removal of the respective heat shields (a.d.)
4. cutting of the inner bellows using a laser beam or by grinding (a.d.)
5. cutting of the outer bellows by the same method (a.d.)
   or, instead of 4 and 5, cutting of the plate connecting the bellows with the shell segments
6. radial movement of the module to be replaced (manipulator)
7. transport of the defect module into the hot cell (crane)
8. removal of the remaining parts of the destroyed bellows in situ (a.d.)
9. adjustment of the new module (manipulator)
10. welding of the modules (a.d.)
11. helium leak test
12. welding of the heat shields (a.d.)
13. insertion of the limiters (a.d.)

For operations inside the vessel automatic or remotely controlled devices have to be developed since the available access is not sufficient for insertion of a manipulator. This development will be done in collaboration with the remote handling group and industry /16/ and comprises devices for:

- inspection of the inner surface of the vessel
- helium leak testing and localization of leaks
- positioning and clamping of other devices for
  - cutting, rewelding and replacement of the heat shield elements
  - cutting and rewelding of the vessel units
  - small repairs by welding - since all vacuum welds are accessible from inside.

The small access and the presence of the large-area limiter considerably restrict the scope for mounting the limiter elements (approx. 10.000) by hand. Besides there is always the danger of damage or getting the limiter or vessel dirty.

Development of an automatic device which may overcome these problems has therefore been started. It should be capable for remote handling and operation in an inert gas atmosphere. As shown in Fig. 23, a guiding disc has to be inserted inside the vessel. Its support at the port seems to be sufficient. On this disc a gripping tool oscillates equidistant to the inner vessel surface between the limiter element to be replaced and a magazine. A prototype of this tool is shown in Fig. 24. It will be actuated by servo motors and pneumatic cylinders and optically remote-controlled using coherent glass fibres or a miniature TV camera. The expected accuracy in positioning is around $\pm$ 2 mm.

6. Conclusion and Outlook to the Next Steps

Summarizing the results obtained from the design studies, stress analysis, and industry, it can be stated that a realization of the vacuum vessel of ZEPHYR with Δ = 9 cm is possible. The condition for that is a magnet suitably designed to support and assemble the vessel, this being a complication of both components that one has to live with.

The design so far is based on static stress analysis. Consideration of low cycle fatigue requirements and of the dynamic nature of the forces at disruption may result in some changes. If necessary, the stresses can be reduced by the introduction of additonal supports and/or by a larger thickness of the bellows (the latter would lower the toroidal electrical resistance).

The next step in the development of the vessel is the freezing of the design parameters. Optimization of the design and study contracts to industry have to follow. This will provide the material for tendering.

The final decision about the material for the limiter mushrooms can be postponed somewhat. However, collection of relevant data is urgend in order to get the basis for a decision in due time.

Appendix

Magnetic Loads Caused by the Poloidal Eigenmode

On a vacuum vessel composed of wedge-shaped shell and bellows sectors eigenmodes of only poloidal currents are excited by time varying toroidal magnetic fields. The ground mode of them, i.e. the poloidal mode with the largest time constant, dominates and only it will be considered here.

The inductive coupling between the shells and bellows is close but not ideal. Therefore, a small part of the toroidal magnetic flux of the ground mode penetrates the surface of each shell and bellows sector causing a toroidal field ripple. The poloidal current density on each shell or bellows sector varies in toroidal direction. For the geometry of the ZEPHYR vacuum vessel the stray flux of the toroidal magnetic field through the vessel wall is small and the toroidal distribution of the poloidal current density was assumed to be constant along each shell or bellows sector, e.g. the shell and bellows sectors are assumed to be ideally coupled.

The pressure exerted on the vessel by the decay of the diamagnetic plasma current during a disruption is derived in the following under this assumption. The pressure caused by the rise or decay of the main field, i.e. eq. (2) of the main text, is obtained in the same way by replacing the exponential change of the flux in (A.1) and (A.2) by a linear one.

The diamagnetic plasma currents decay exponentially such that their toroidal flux can be represented by $\tilde{\Phi}_T \left(1 - e^{-t/\tau_p}\right)$, $\tilde{\Phi}_T$ being given by eq. (5) of the main text. The induced poloidal vessel currents on the shell, I_s, and on the bellows, I_B, are described by two simple differential equations

(A.1)
$$\frac{dI_s}{dt} + \frac{dI_B}{dt} + I_s \cdot \frac{R_s}{L_o} = \frac{|\tilde{\Phi}_o|}{\tau_p \cdot L_o} \cdot e^{-\frac{t}{\tau_p}}$$

(A.2)
$$\frac{dI_B}{dt} + \frac{dI_s}{dt} + I_B \cdot \frac{R_B}{L_o} = \frac{\tilde{\Phi}_o}{\tau_p \cdot L_o} \cdot e^{-\frac{t}{\tau_p}}$$

with the solutions

$$I_B(t) = \frac{R_s}{R_B + R_s} \cdot I_{POL}(t) \qquad I_s(t) = \frac{R_B}{R_B + R_s} I_{POL}(t)$$

and

$$I_{POL}(t) = \frac{\tilde{\Phi}_0}{L_0 \cdot \tau_p} \cdot \frac{1}{[1/\tau_p - 1/\tau_G]} \cdot \left[e^{-t/\tau_G} - e^{-t/\tau_p} \right]$$

R_B = poloidal resistance of all bellows sectors

R_S = poloidal resistance of all shell sectors

$1/\tau_G = R_B \cdot R_S / (R_B + R_S) L_0$ poloidal time constant of the vacuum vessel.

L_0 = vessel inductance neglecting toroidal field ripple

I_{POL} = poloidal vessel current

The electromagnetic pressure load on a shell sector (which also depends on the position along R) is given by

$$(A.3) \quad p_s(t) = \frac{I_s(t)}{\ell_s \cdot N} \cdot B_T = \langle p \rangle(t) \cdot \frac{(\ell_B + \ell_s)}{\ell_s} \cdot \frac{R_B}{(R_B + R_s)}$$

(B_T being the toroidal field)

and on a bellows sector by

$$(A.4) \quad p_B(t) = \frac{(\ell_B + \ell_s)}{\ell_B} \cdot \frac{R_s}{(R_B + R_s)} \cdot \langle p \rangle(t)$$

$\ell_{B,S}$ = toroidal length of single bellows or shell sector at R, and

$$(A.5) \quad \langle p \rangle(t) = \frac{I_{POL}(t)}{2\pi \cdot R} \cdot B_T$$

is the mean pressure load on the vessel.

The vessel inductivity L_0 is connected with the toroidal magnetic flux Φ_{T_V} of the main field B_T (R) by

$$\Phi_{T_V} = \frac{2\pi}{\mu_0} \cdot R \cdot B_T(R) \cdot L_0$$

By inserting this expression into equation (A.5) one can verify the equivalence of equation (A.5) and equation (3) of the main text.

Equations (3) and (4) are valid for nearly any time constant of the toroidal magnetic fields inside the vessel. Only in the case $\tau_p << \tau_\sigma$ correction terms in the equations (1) and (2) have to be intoduced which take into account the small toroidal stray flux.
At the time t = 0 the electromagnetic pressure load is equally distributed along the toroidal direction of the vacuum vessel as described by $< p > (t)$.
The transition from $< p > (t)$ to $p_\beta (t)$ and $p_s (t)$ occurs in a time much shorter than τ_σ .

References

/1/ "Compact Ignition Experiment", Status Report prepared by IPP Garching and CNEN Frascati, September 1978

/2/ H. Kotzlowski, K.F. Mast, H. Preis: Report IPP 1/175 (Nov. 79)

/3/ H. Kotzlowski, K.F. Mast, H. Vernickel, J. Nucl. Mat. 94/95 (1980) in press

/4/ A. Boschi, C. Ferro, A.Orsini: Fusion Technology 1978, Vol. 2, p. 855 (Proc. 10th SOFT) Pergamon Press 1978

/5/ D.B. Albert: Report IPP III/54 (Jan. 1980)

/6/ K.F. Mast: Report IPP 1/174 (Nov. 1979)

/7/ A.W. Mullendore, J.B. Whitley, D.M. Mattox, J. Nucl. Mat.94/95 (1980) in press

/8/ R.A. Langley, L.C.Emerson, J.B. Whitley, A.W. Mullendore, J. Nucl. Mat. 94/95 (1980), in press

/9/ H.W. Carslaw, J.C. Jaeger, "Conduction of heat in solids", Oxford, Clarendon Press, 1959

/10/ R. Behrisch, J. Nucl. Mat. 94/95 (1980), in press

/11/ U. Daybelge, B.K. Bein - to be published

/12/ J.F. Dylla, J. Nucl. Mat. 94/95 (1980), in press

/13/ F. Brossa, J. Bohdansky, J. Roth, A.P. Martinelli, J. Nucl. Mat. 94/95 (1980) in press

/14/ U. Brossmann, J.E. Gruber, W.D. Haubenberger, O. Jandl, F. Mast, M. Söll B. Streibl, Report IPP 1/176

/15/ K. Lackner u.a. Internal ZEPHYR Report No. 23

/16/ C. Andelfinger, E. Lackner, M. Ulrich, G. Weber, H.-B. Schilling, Internal ZEPHYR Report No. 11 (May 1980)

/17/ W. Köppendörfer, Internal ZEPHYR Report No. 21

Inner diameter	150	cm
Outer diameter *	570	cm
Height *	160	cm
Poloidal circumference	580	cm
Toroidal circumference at R = 202 cm	640	cm
Poloidal cross-section	2,4	m^2
Volume	27	m^3
Internal wall area (smooth)	62	m^2
Internal wall area (total)	≈ 200	m^2
Dead weight *	11000	kg
Dead weight (total)	≈ 18000	kg
Toroidal electr. resistance	0,4	mΩ
Poloidal electr. resistance	0,04	mΩ
Material	Inconel 625	

*without ports

Table I: Parameters of the vacuum vessel

Experiment	I_{Plasma} MA	B_{Tor} T	B_{Pol} T	Δ^* cm	R_{Tor} mΩ	double walled	thermal shield	large area limiter	noncircular shape	external supporting	completely welded - no bolted and sealed joints	operation at 80 K	separate cooling	remote handling
JT 60	2,7	4,5	0,4	23	1,3				X					
TFTR	2,5	5,2	0,42	18	3,0		X	X					X	X
JET	3,8	2,7	0,5	21	0,5	X			X					X
ZEPHYR	3,7	9,1	1	9	0,4	X	X	X	X	X	X	X	X	X

Δ^* : distance plasma - coils at the throat of the magnet

Table II: Comparison of parameters and specific features of large tokamak vacuum vessels

loading case	max Press. MPa	load durat.	F_R kN	F_Z kN
Atmospheric pressure	0,1	stat.	16	10
Toroidal field rise / drop	0,42	7 s	± 14	± 27
Plasma disruption - saddle currents	7	2,2 ms	± 32	± 80
Plasma disruption - toroid. currents	0,8	2,2 ms	140	35
Heating by neutrons $\Delta T_{pol} = 90$ K	–	15 min	2	16
$T_{Magnet} - T_{vessel} = -200$ K 1)	–	stat.	6	58
$\Delta T_{vessel\ wall} = T_i - T_a = 50$ K 2)	–	5 min	4	12
Heating by plasma losses				
Movements of the magnet				

1) during normal operation

2) after discharge until cooling becomes efficient

Table III: Reaction forces at the vertical and radial support of the vessel for different loading cases (calculated for the double wall design A = 3,5; k = 1,5; R_c = 126 cm, r_c = 36 cm)

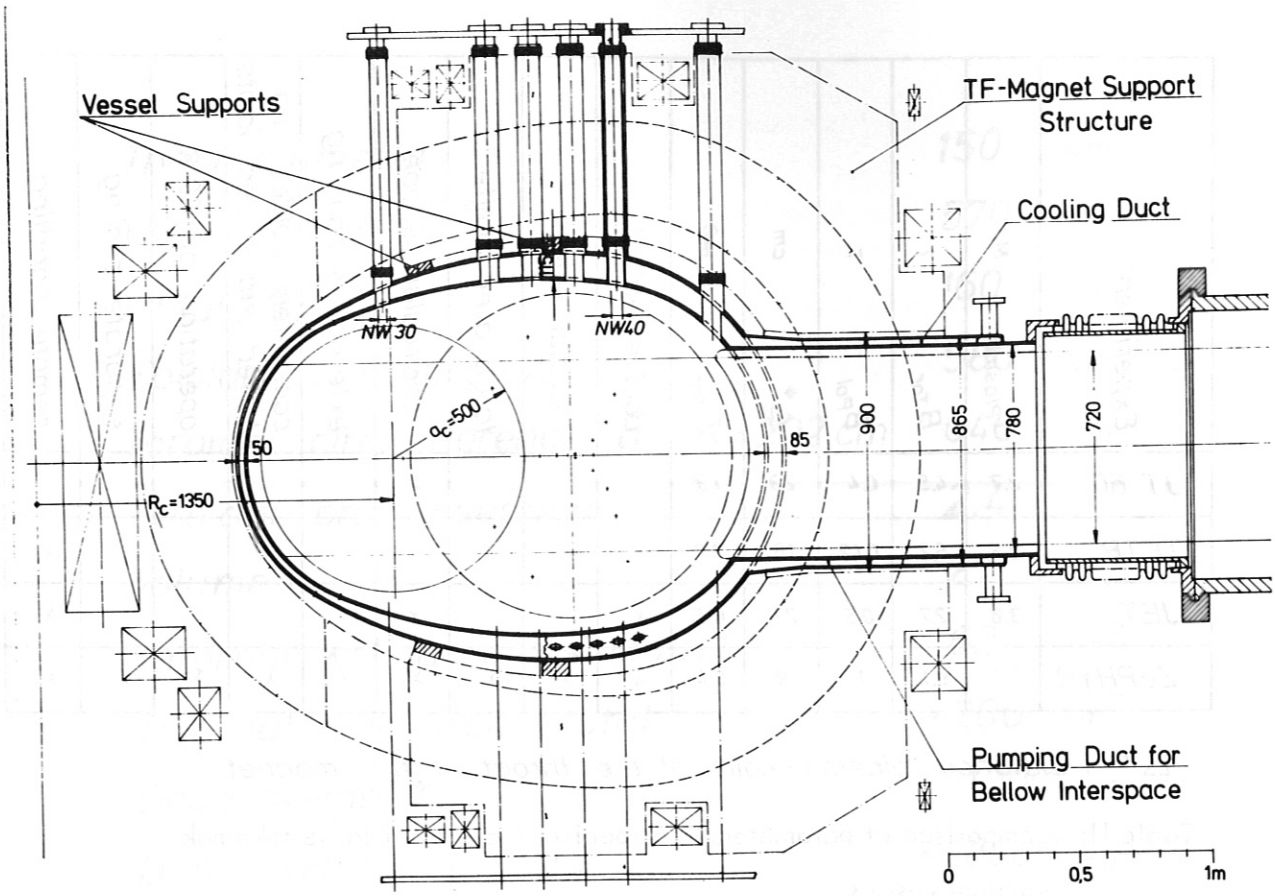

Fig. 1 Vertical section of the vacuum vessel

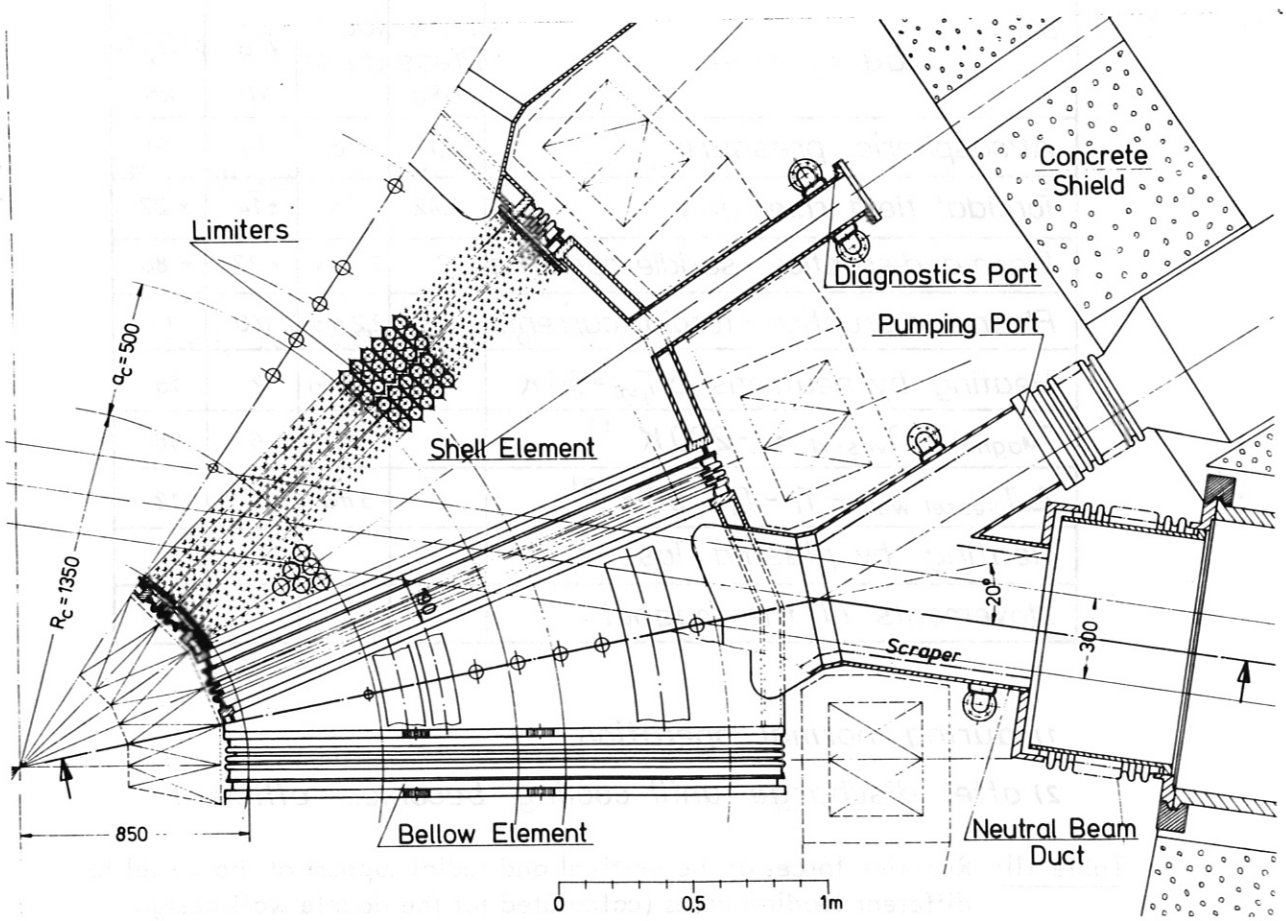

Fig. 2 Equatorial section of the vacuum vessel

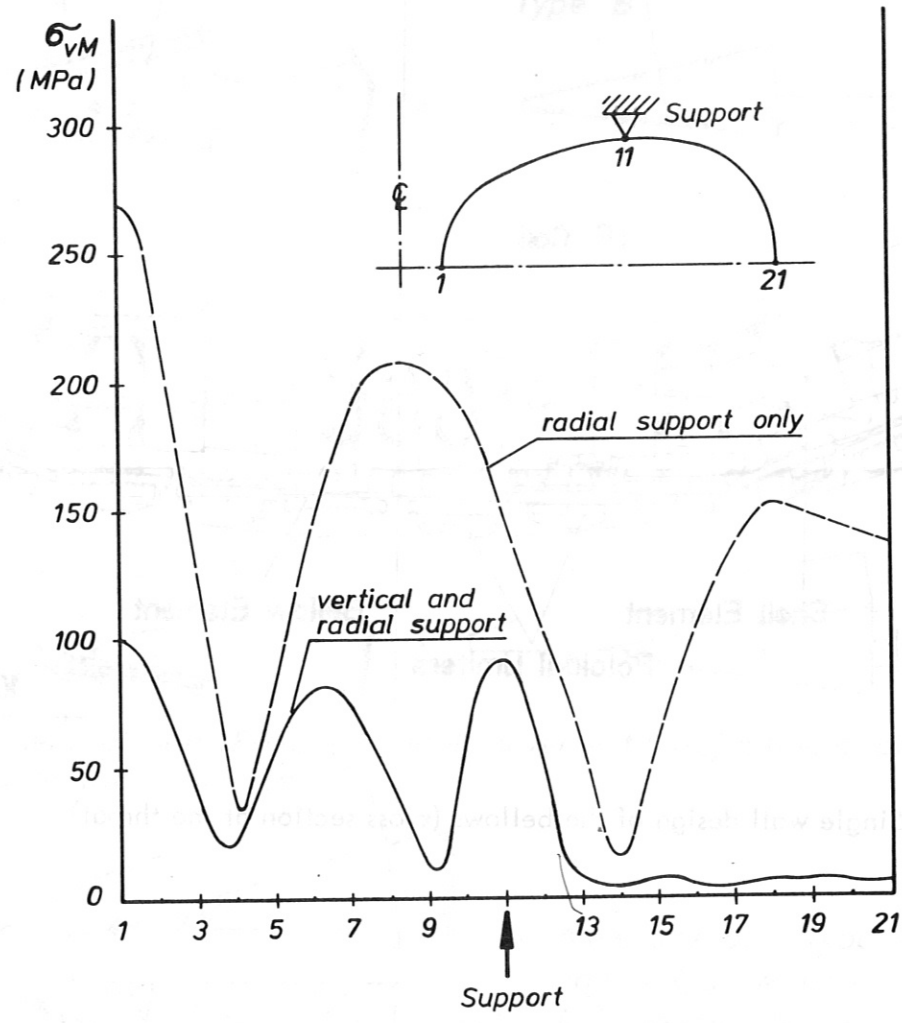

Fig. 3 Stress reduction in the vessel shell when supported vertically (calculated for the double wall design A = 3,5; K = 1,5; R_c = 126 cm; r_c = 36 cm; load case: electromagnetic forces during B_{tor}-rise)

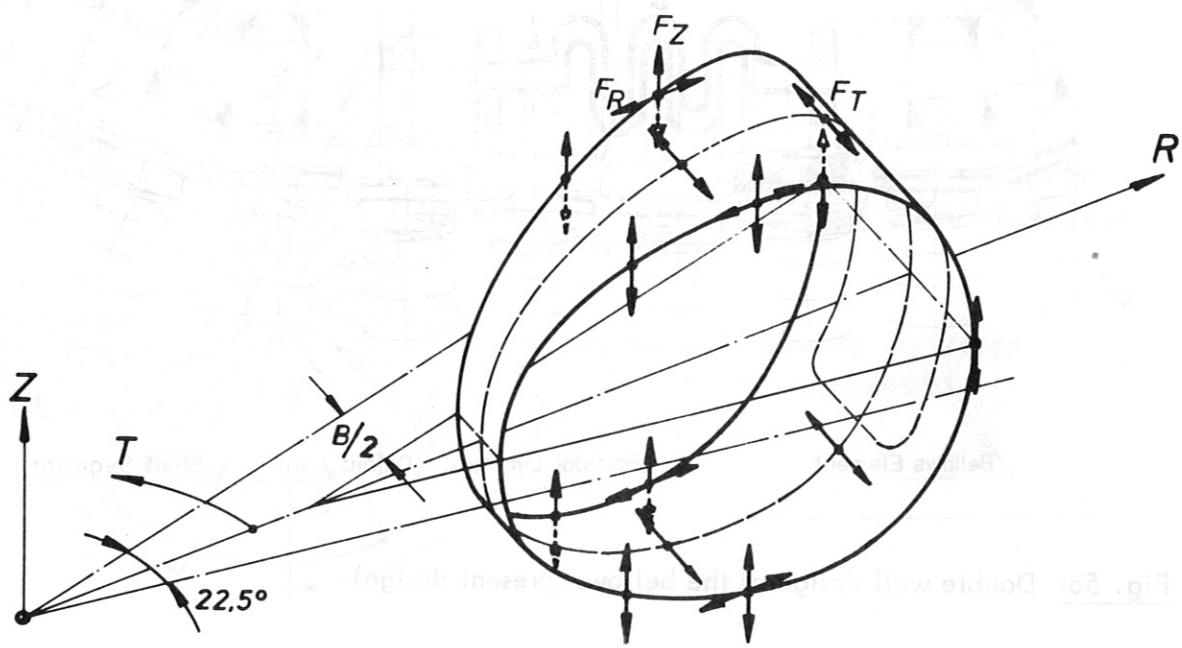

Fig. 4 Supports of a shell element and direction of reaction forces to be transmitted

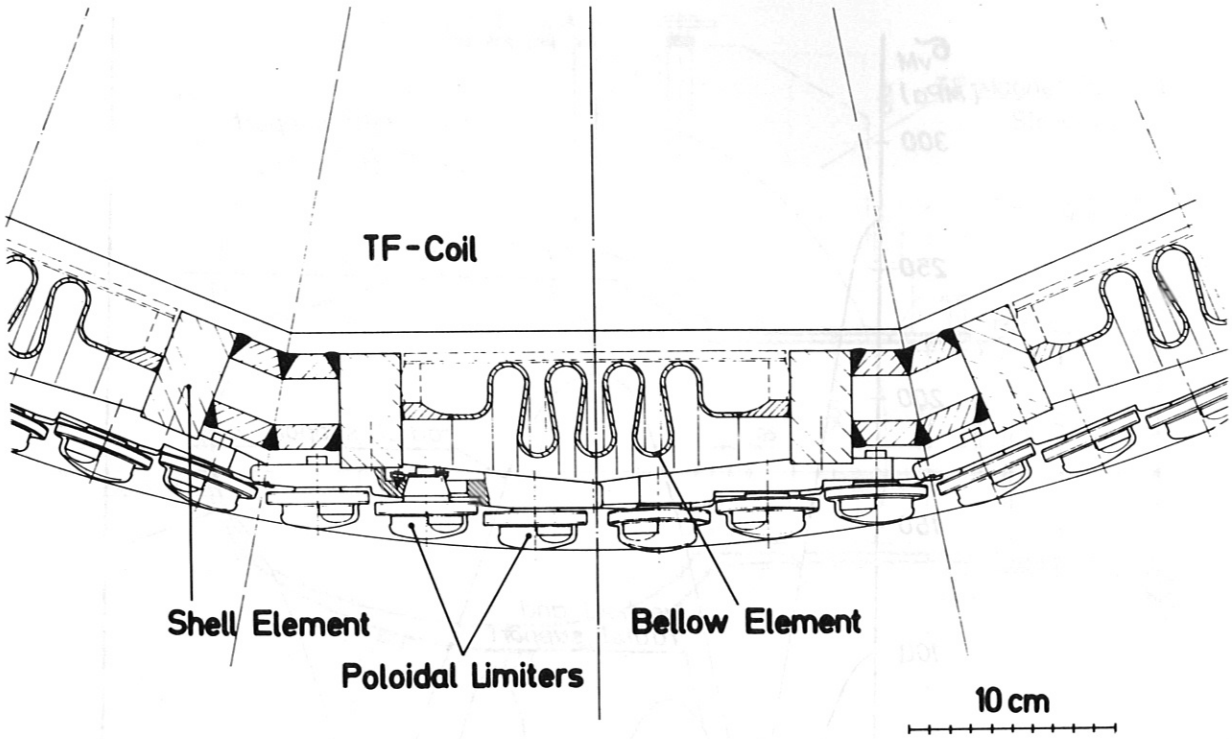

Fig. 5a: Single wall design of the bellows (cross section at the throat)

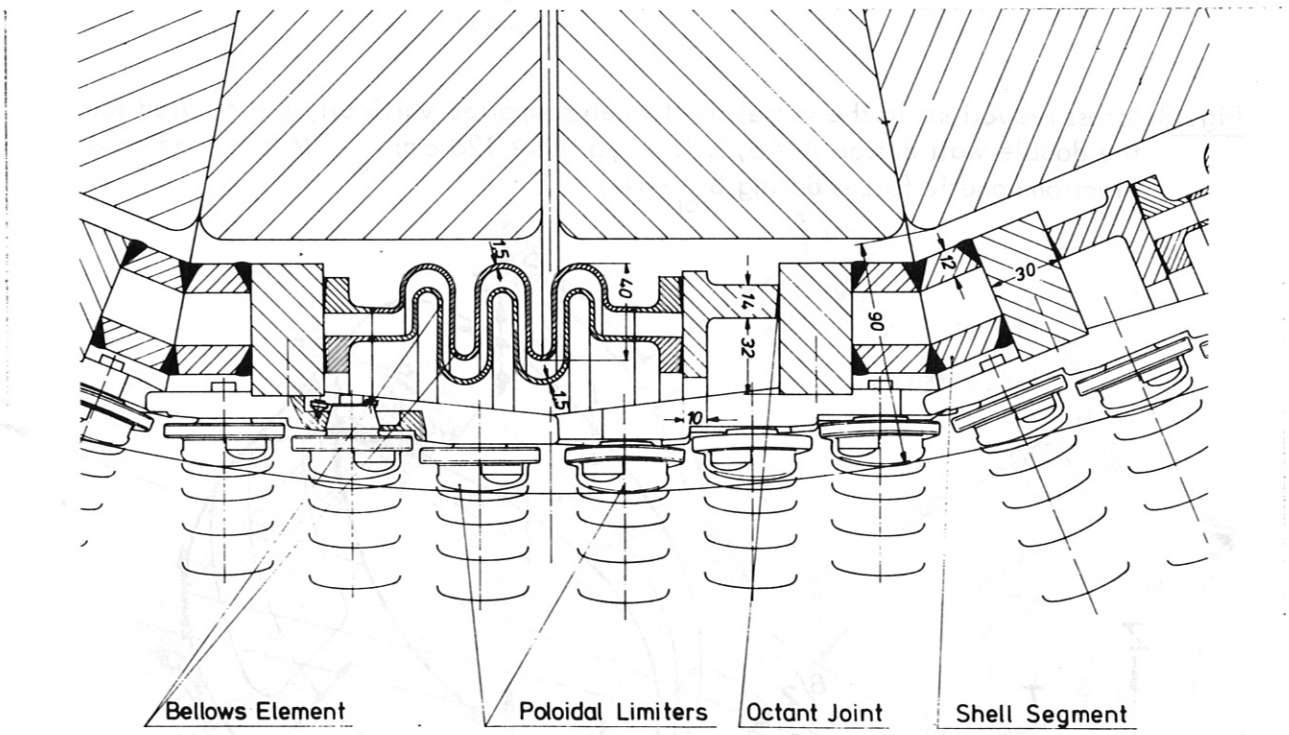

Fig. 5b: Double wall design of the bellows (present design)

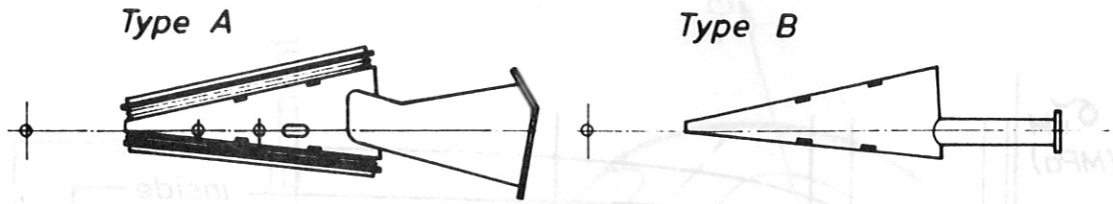

1. Assembly and test of the vessel units

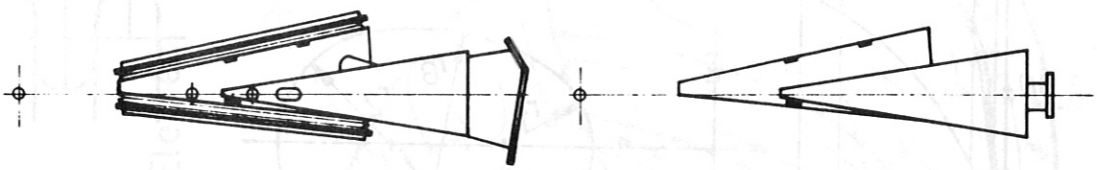

2. Attachment of the wedges (Type B vertical, Typ A radial movement)

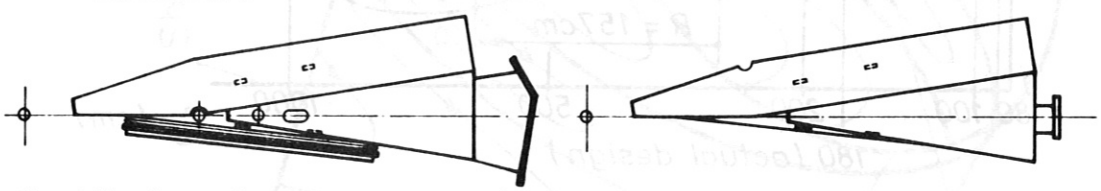

3. Attachment of one TF-coil (toroidal movement), adjustment and locking of the supports

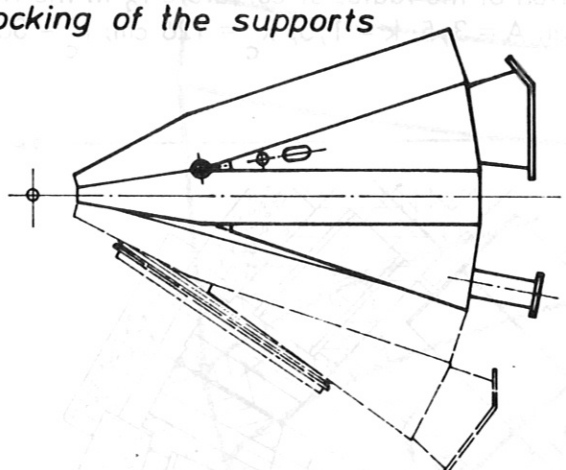

4. Assembly of a Type B and a Type A units to 45°-segments

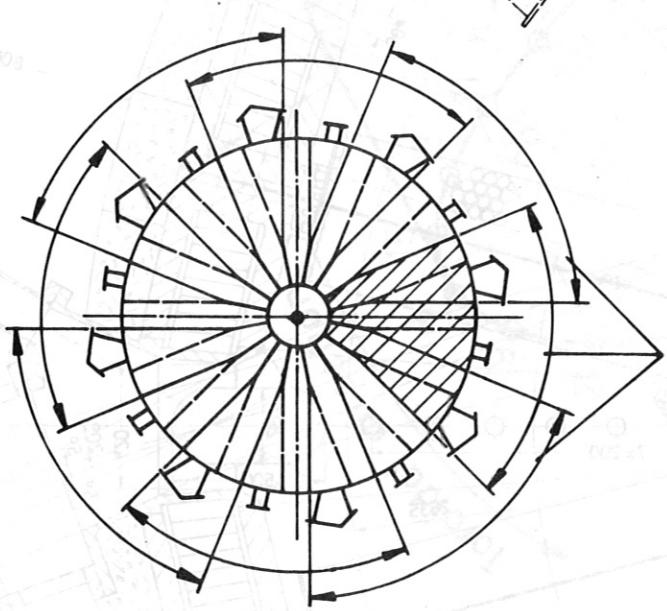

5. Assembly to a complete torus and final leak test

exchangeable modules (67,5°-segments)

Fig. 6 Assembly process of vessel plus magnet

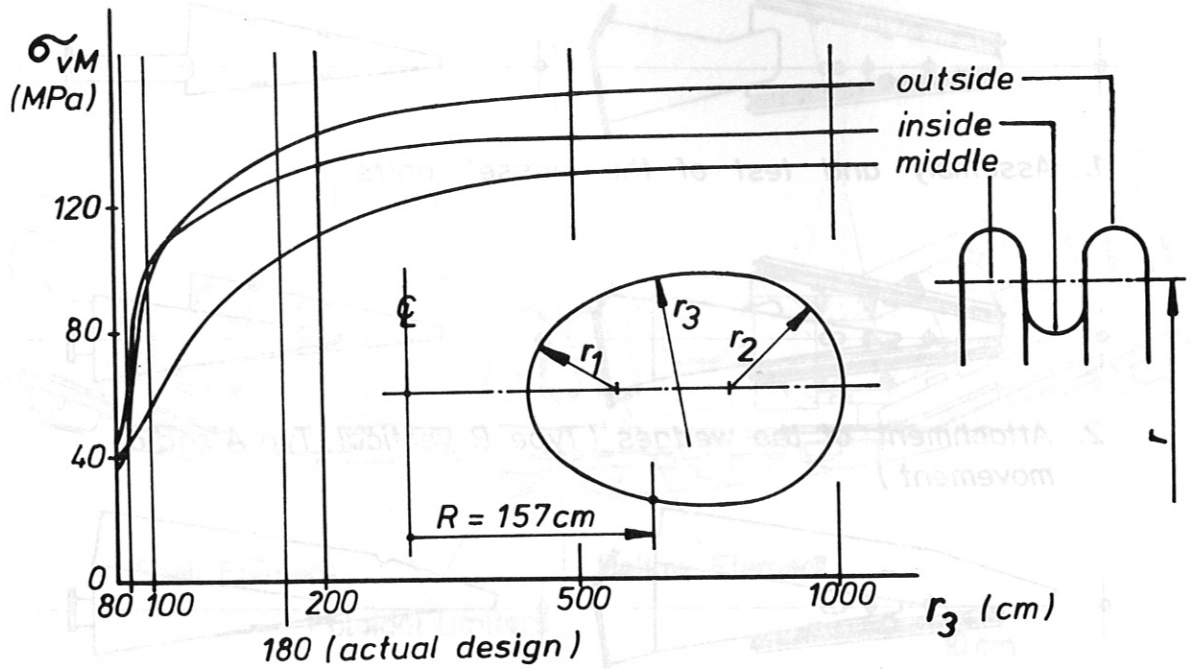

Fig. 7 Stresses in the bellows as function of the radius of curvature r_3 in the flat portion (calculated for the vessel design A = 3,5; k = 1,5; R_c = 126 cm; r_c = 36 cm, load case atm. pressure)

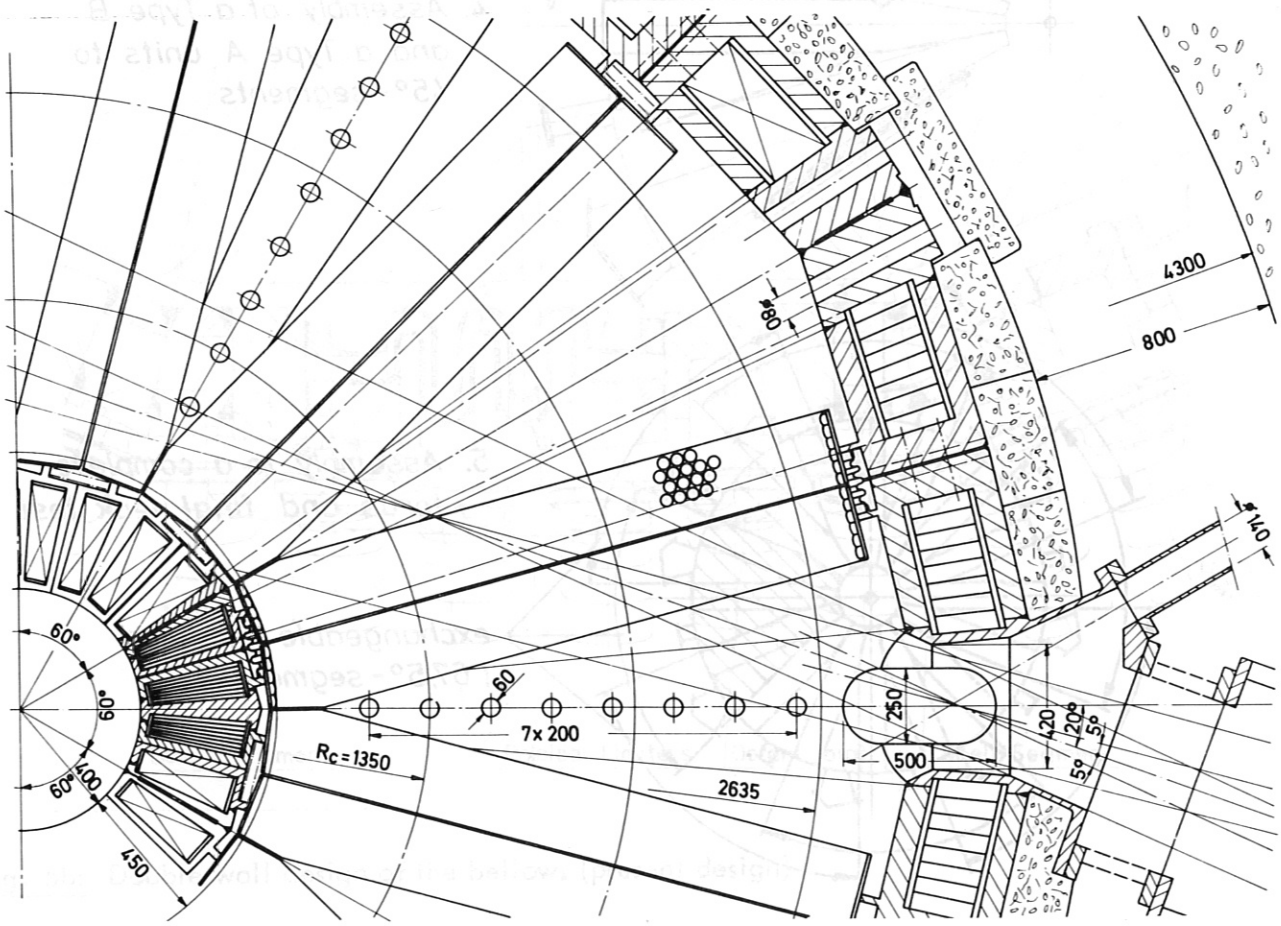

Fig. 8 Integration of the vessel into the magnet (alternative concept of the vessel)

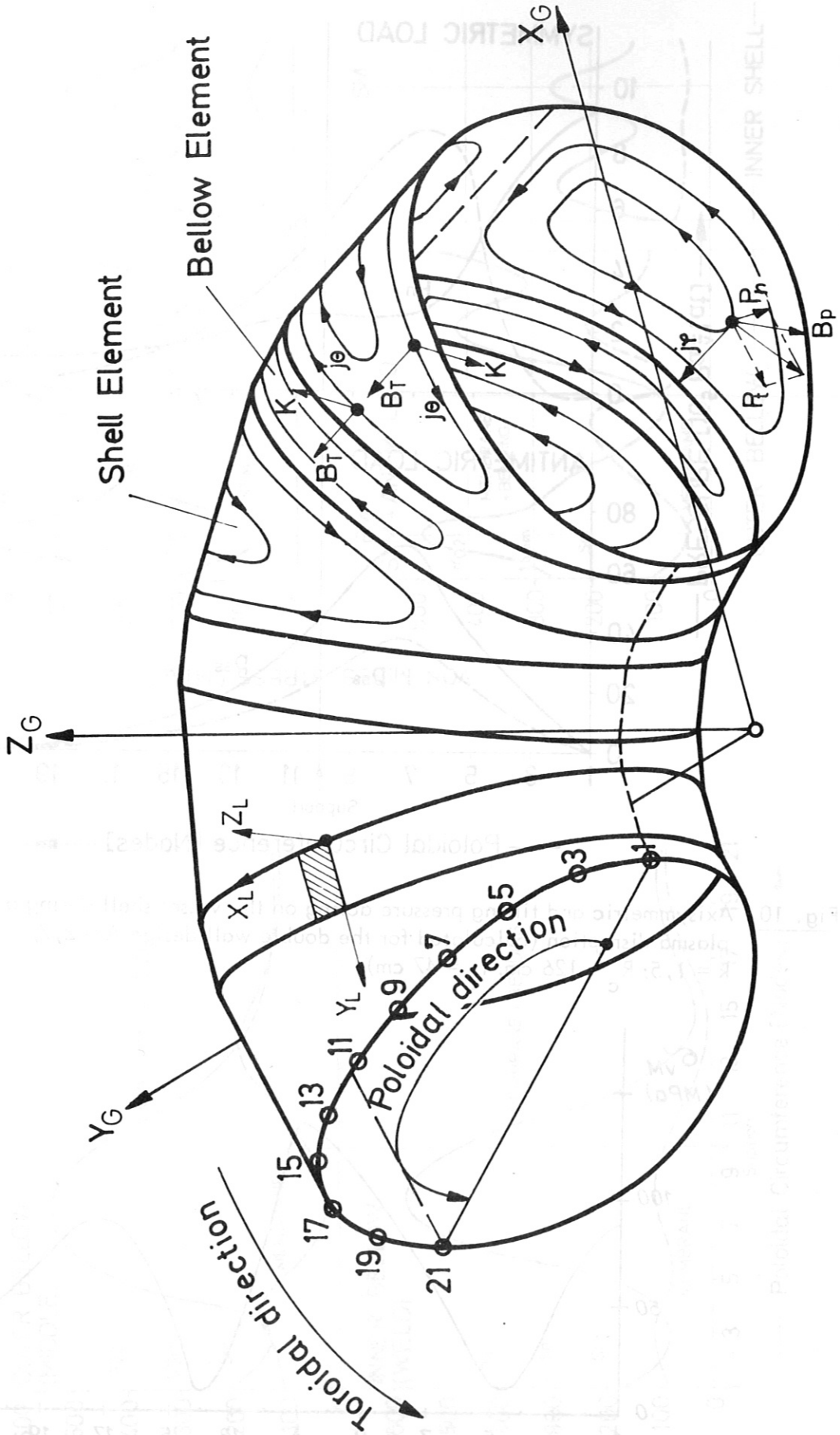

Fig. 9 Saddle currents on shell and bellows elements

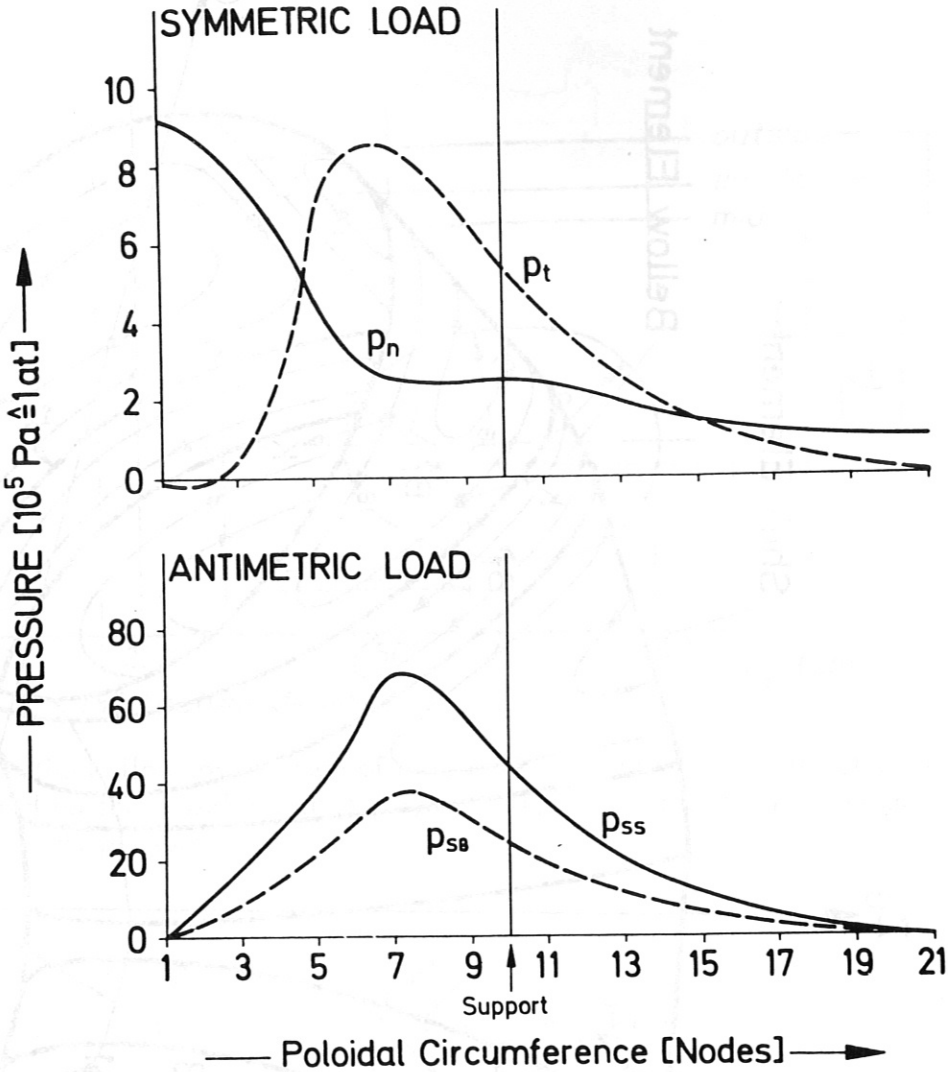

Fig. 10 Axisymmetric and tilting pressure acting on the vessel shell during a hard plasma disruption (calculated for the double wall design A = 2,7; k = 1,5; R_c = 126 cm; r_c = 47 cm)

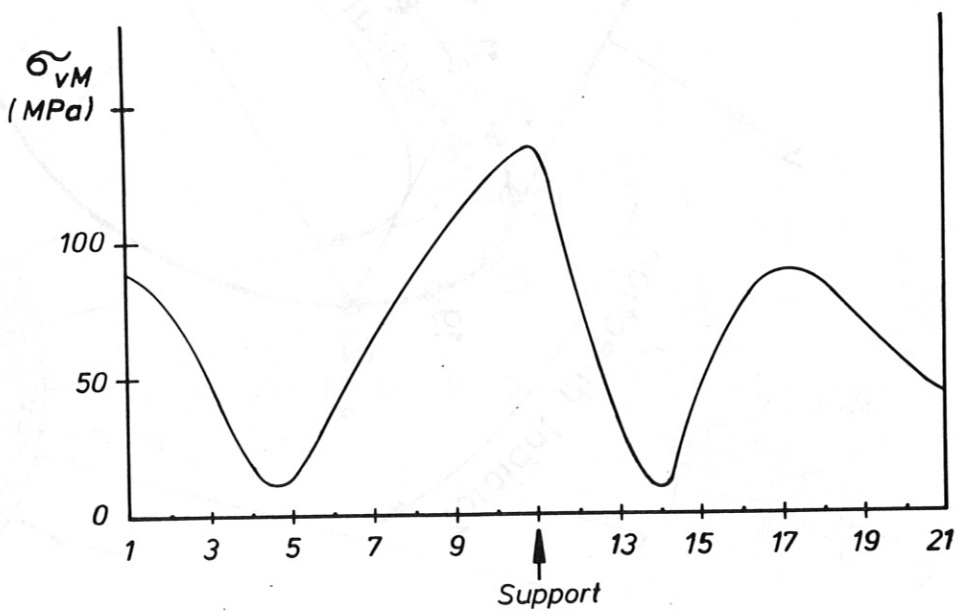

Fig. 11 Stresses in the vessel shell caused by a temperature difference to the magnet of 200 K (calculated for the double wall design A = 3,5; k = 1,5; R_c = 126 cm; r_c = 36 cm)

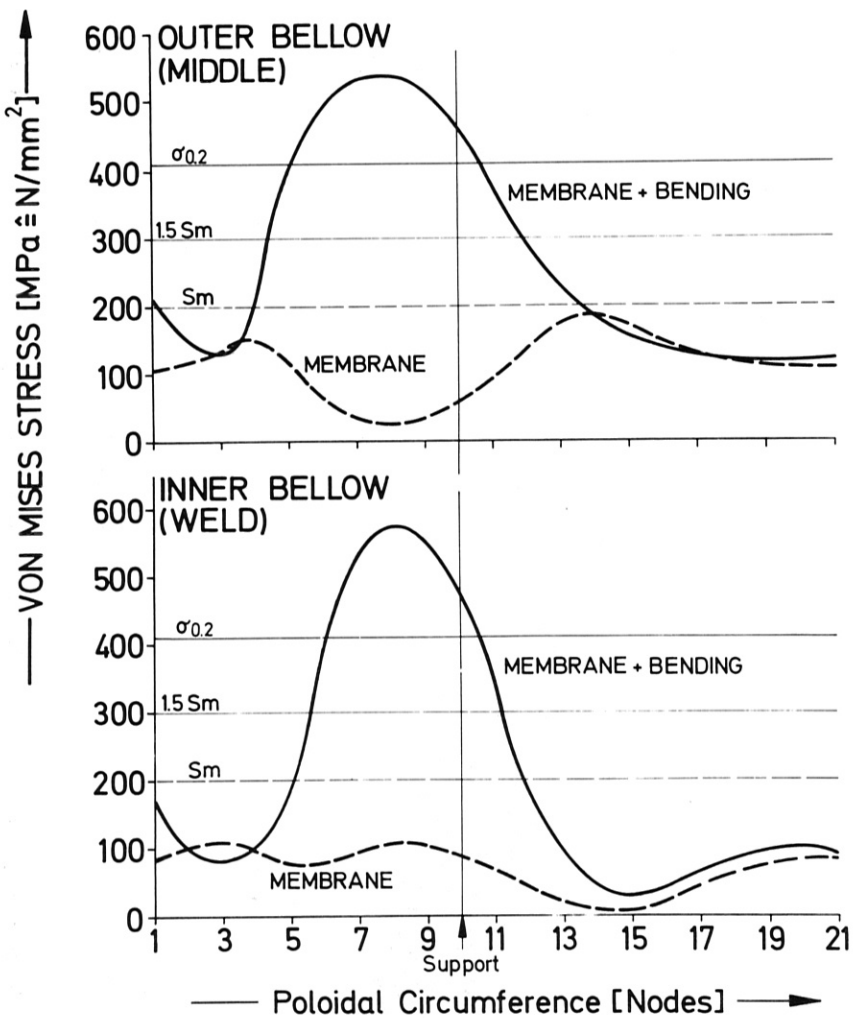

Fig. 12 Stresses in the vessel shell during a hard plasma disruption -distribution along the poloidal circumference (calculated for the double wall design A = 2,7; K = 1,5; R_c = 126 cm; r_c = 47 cm)

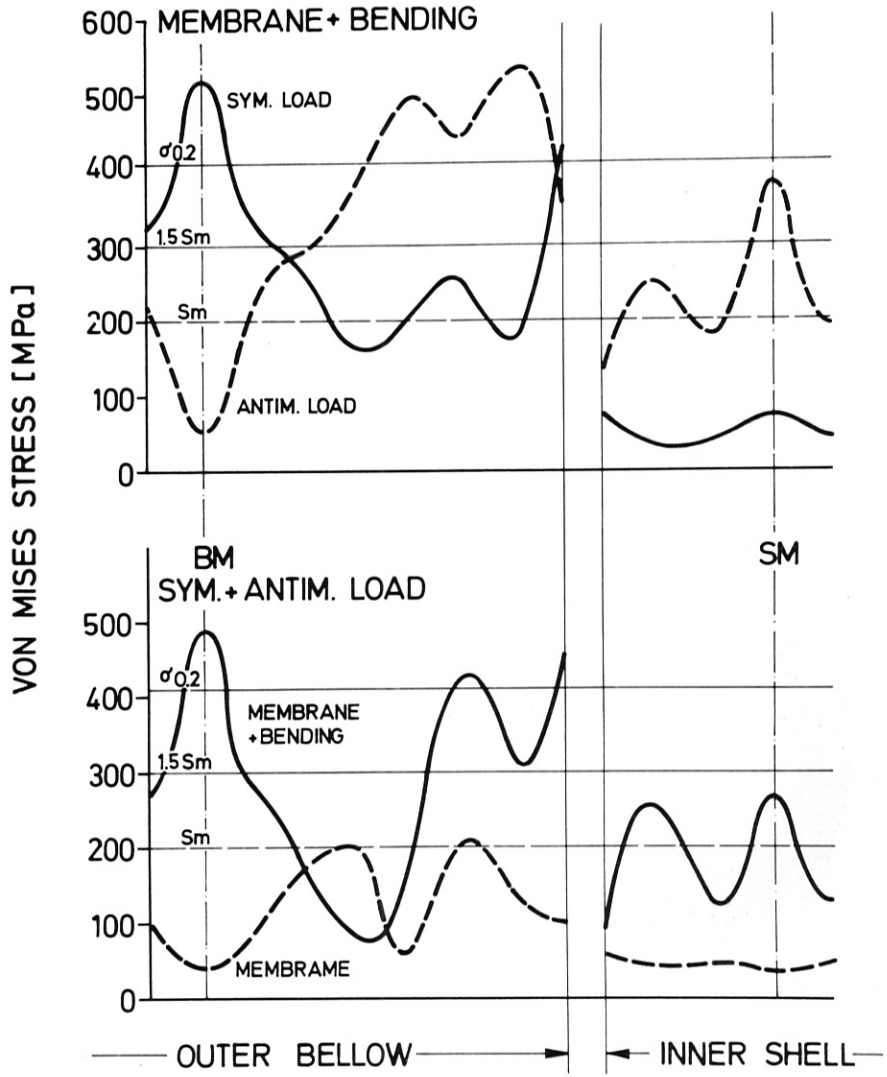

Fig. 13 Stresses in the vessel shell during a hard plasma disruption -distribution along the toroidal circumference (calculated for the double wall design A = 1,7; K = 1,5; R_c = 126 cm; r_c = 47 cm)

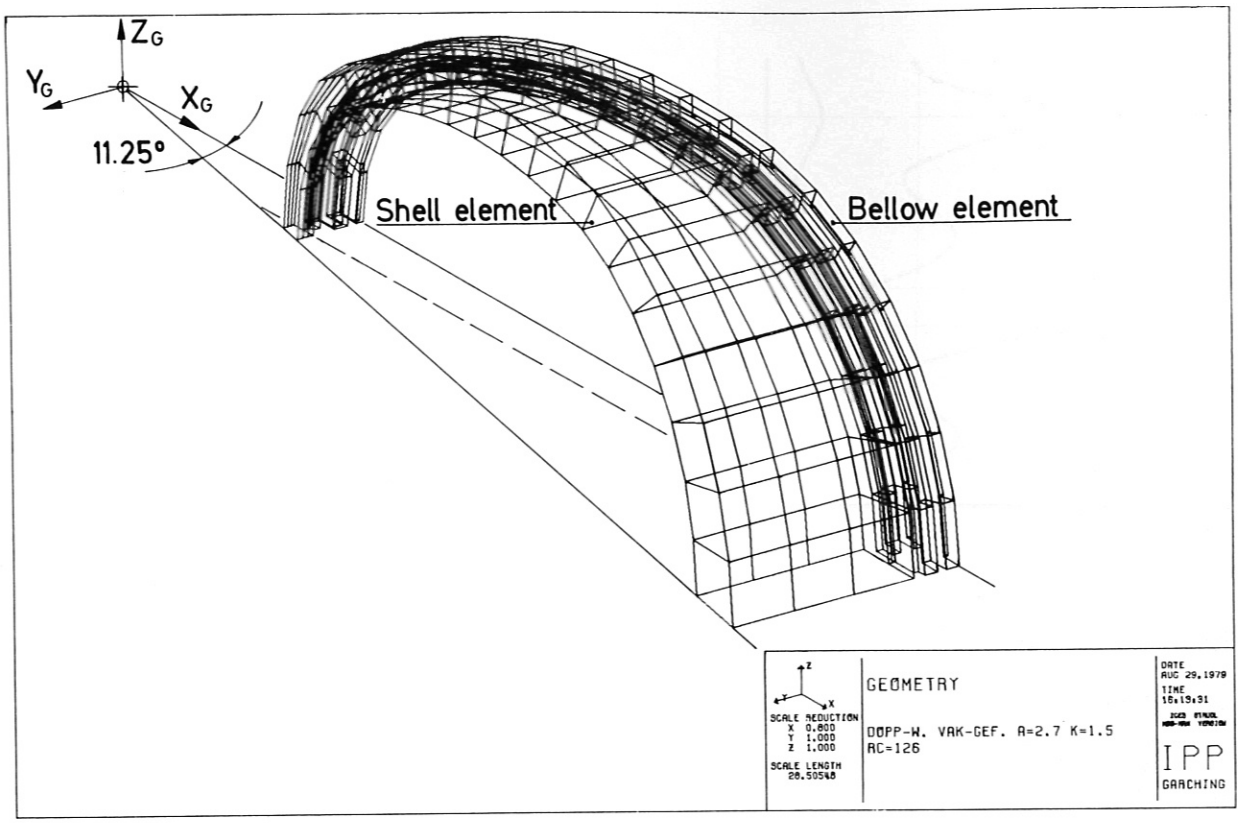

Fig. 14 Isometric view of the FE-mesh for stress analysis

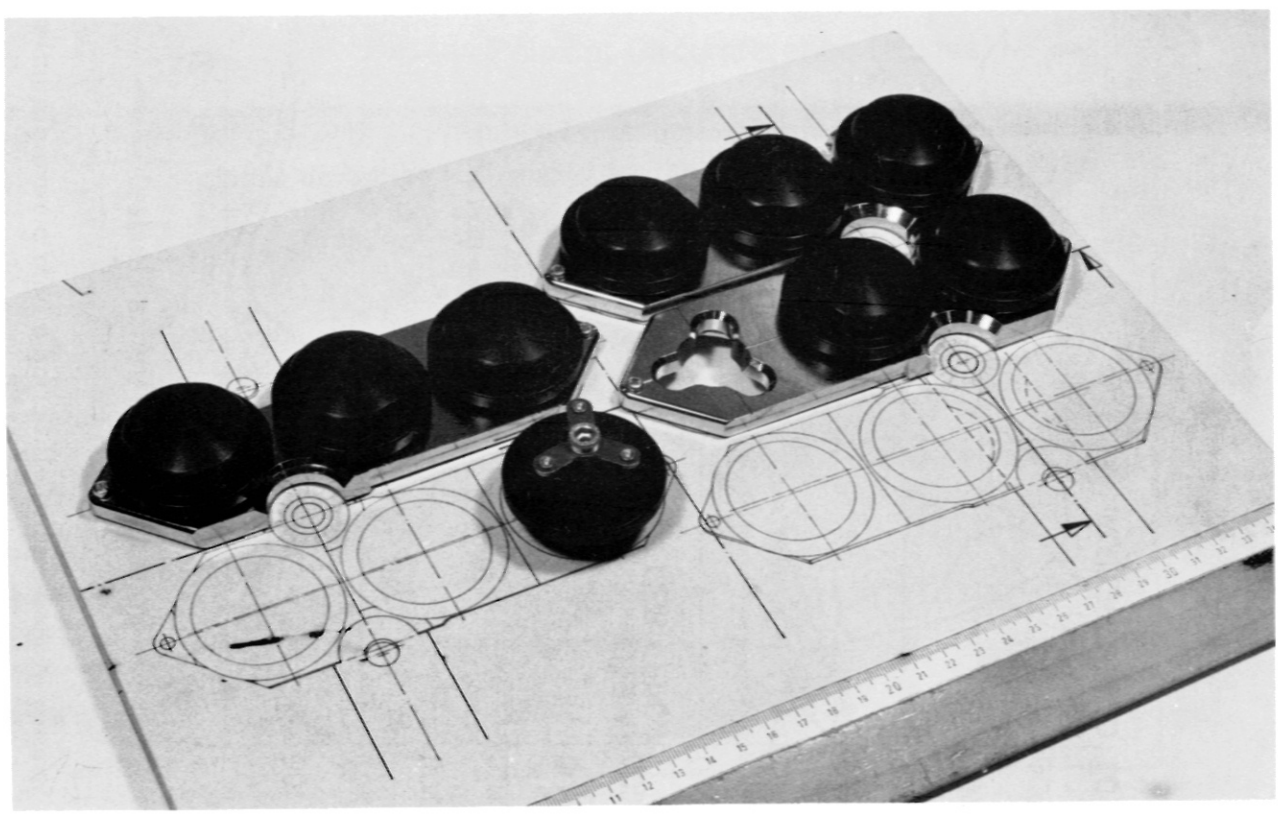

Fig. 15 Arrangement of the heat shields in combination with the limiter elements (at the throat of the magnet)

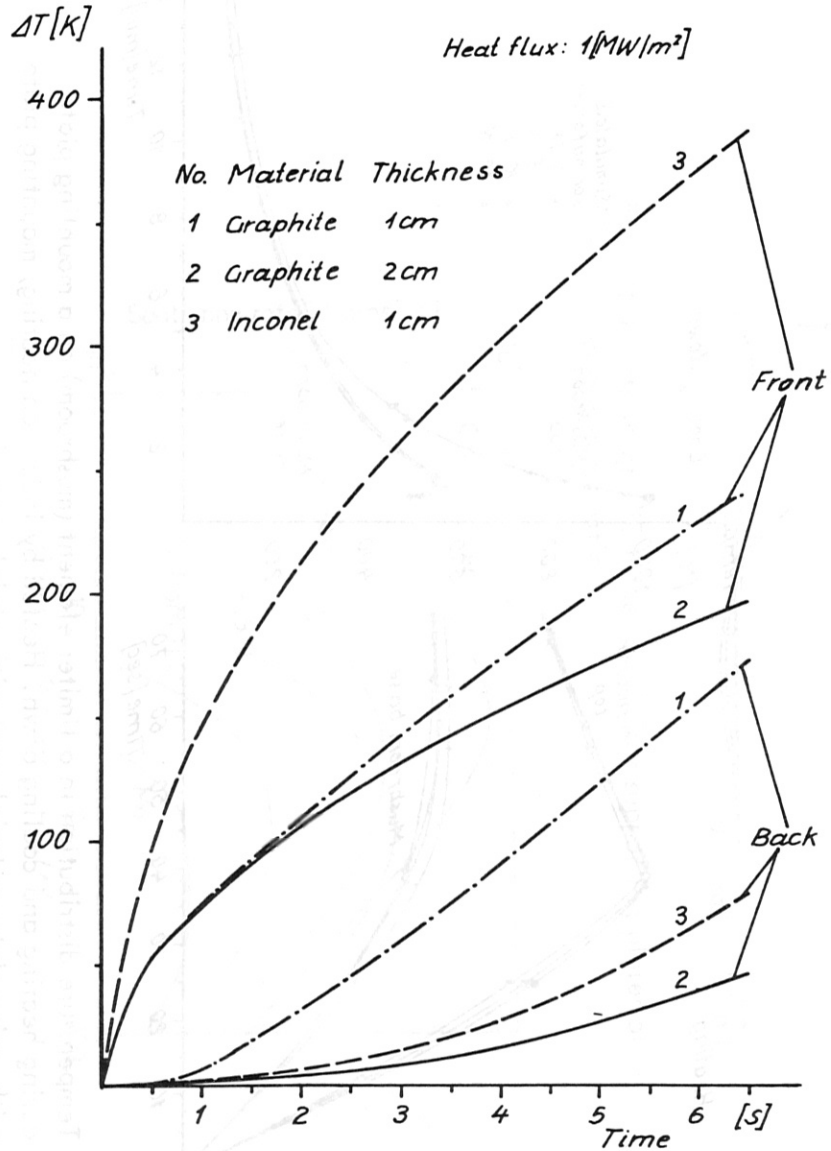

Fig. 16 Temperature rise versus time in slabs of graphite (d = 1 cm and d = 2 cm) and inconel (d = 1 cm) heated by a steady flux of 1 MW/m^2. The temperature rise is proportional to the heat flux. [λ = 15 W/Km, a = $\lambda/\varrho c$ = $4 \cdot 10^{-6}$ m^2/s for Inconel, λ = 65 W/Km, a = $1{,}9 \cdot 10^{-5}$ m^2/s for graphite]

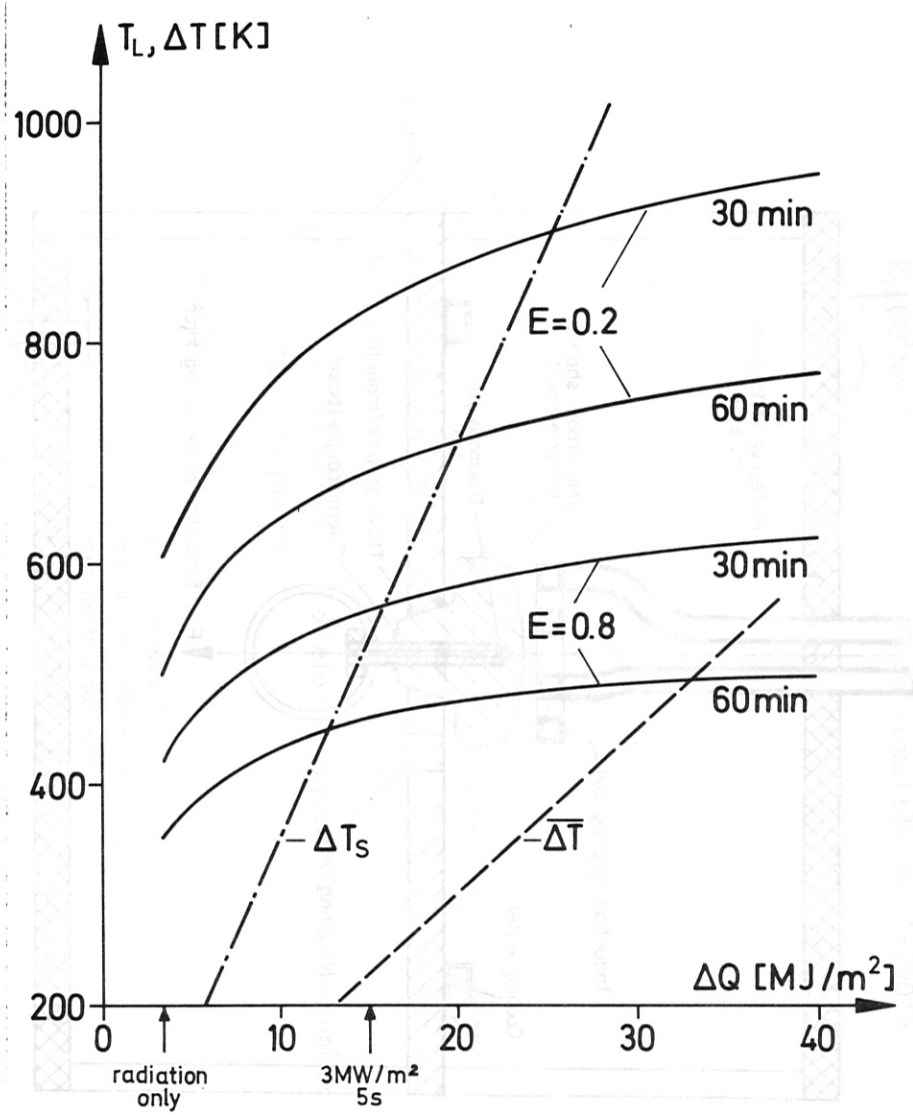

Fig. 17 Calculated temperature of the radiation cooled 2 cm thick limiter (in steady state) at the end of a cooling time of 30 (60) min. as function of energy input during the shot. E is the emissivity. Also indicated are the average and the surface temperature increase at the end of the discharge.

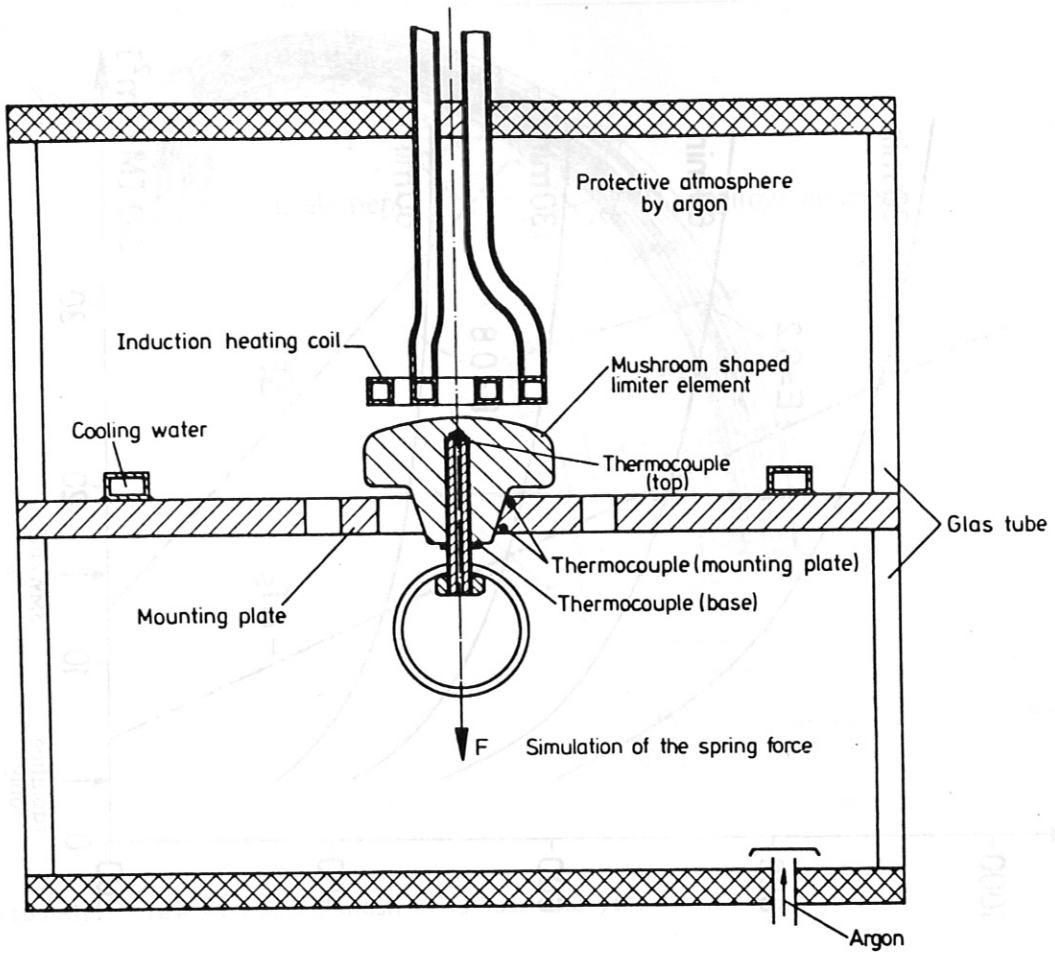

Fig. 18 Arrangement of the limiter elements (mushrooms) in the test equipment for the heating test

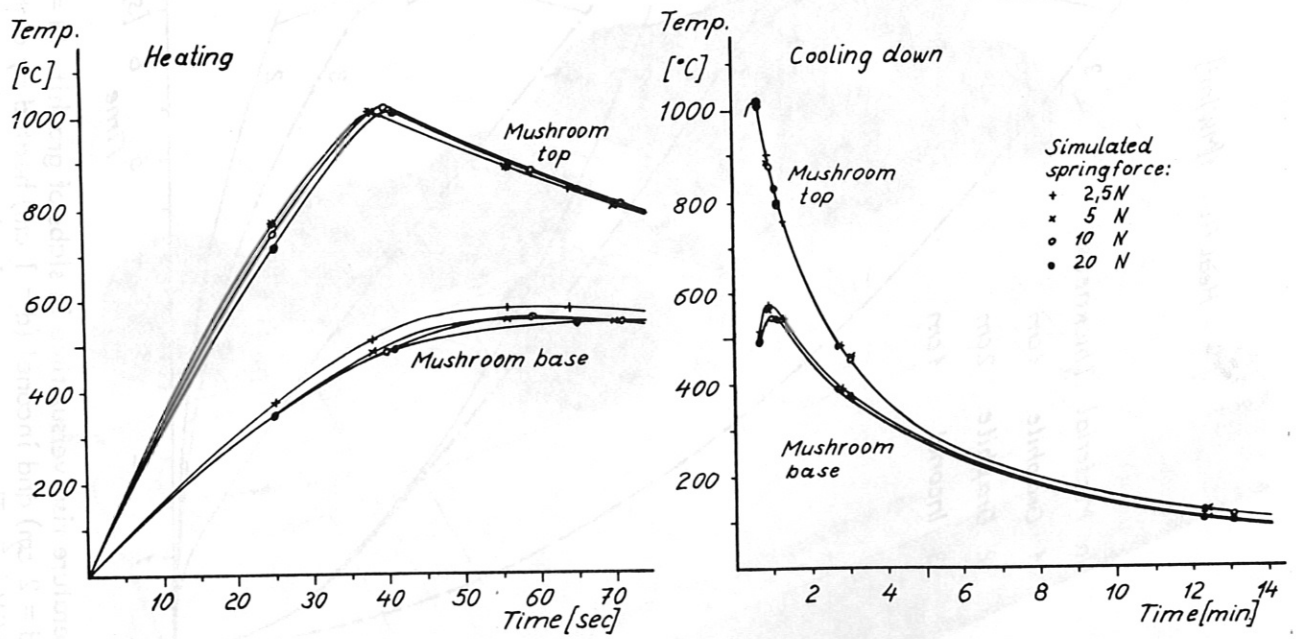

Fig. 19 Temperature distribution in a limiter element (mushroom) on a mounting plate during heating and cooling down. Heated by induction heating; mounting plate with spring slots; material: austenitic stainless steel

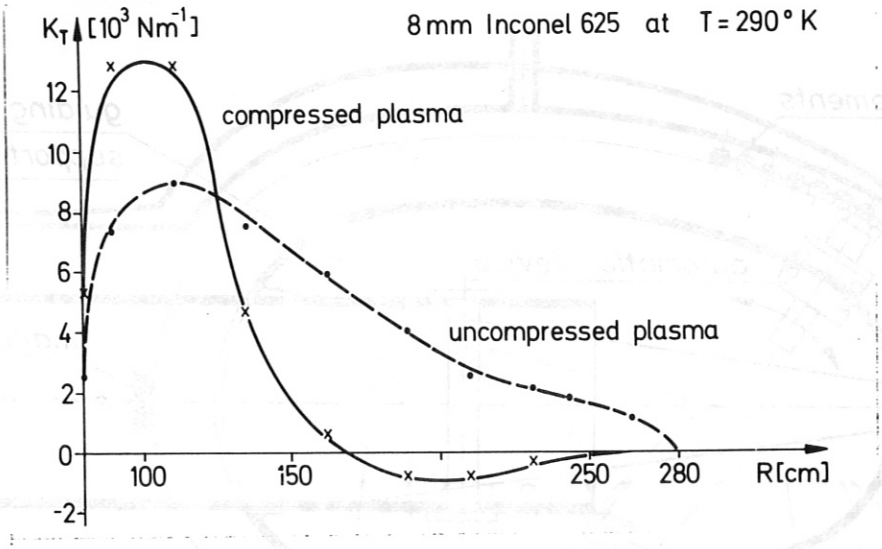

Fig. 20 Poloidal distribution of electromagnetic forces on limiter supporting plates

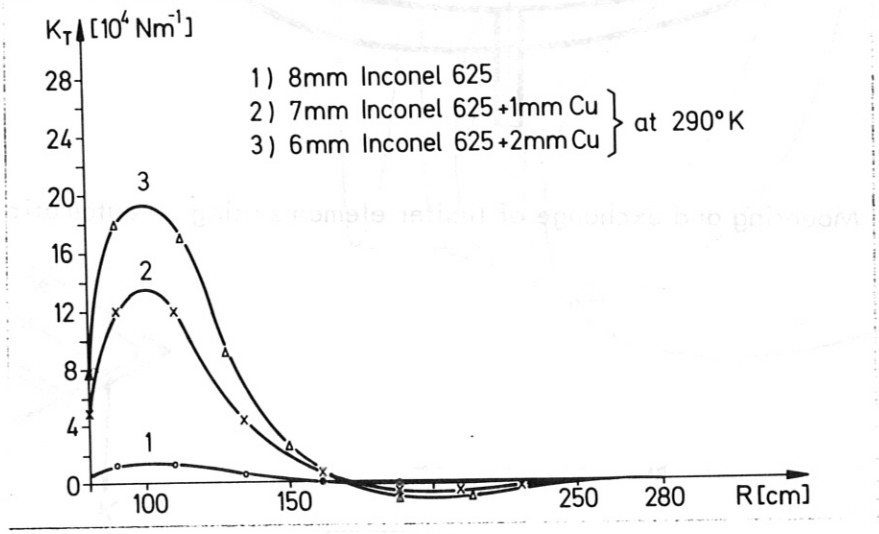

Fig. 21 Electromagnetic forces on limiter supporting plates of various compositions

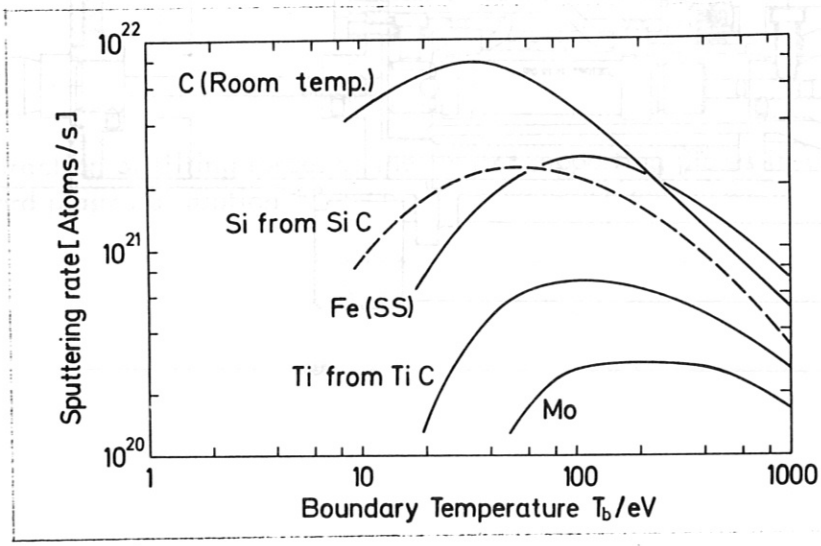

Fig. 22 Sputtering rate coupled with energy transport of 8 MW to the limiter as function of the boundary temperature T_b (for details see /3/)

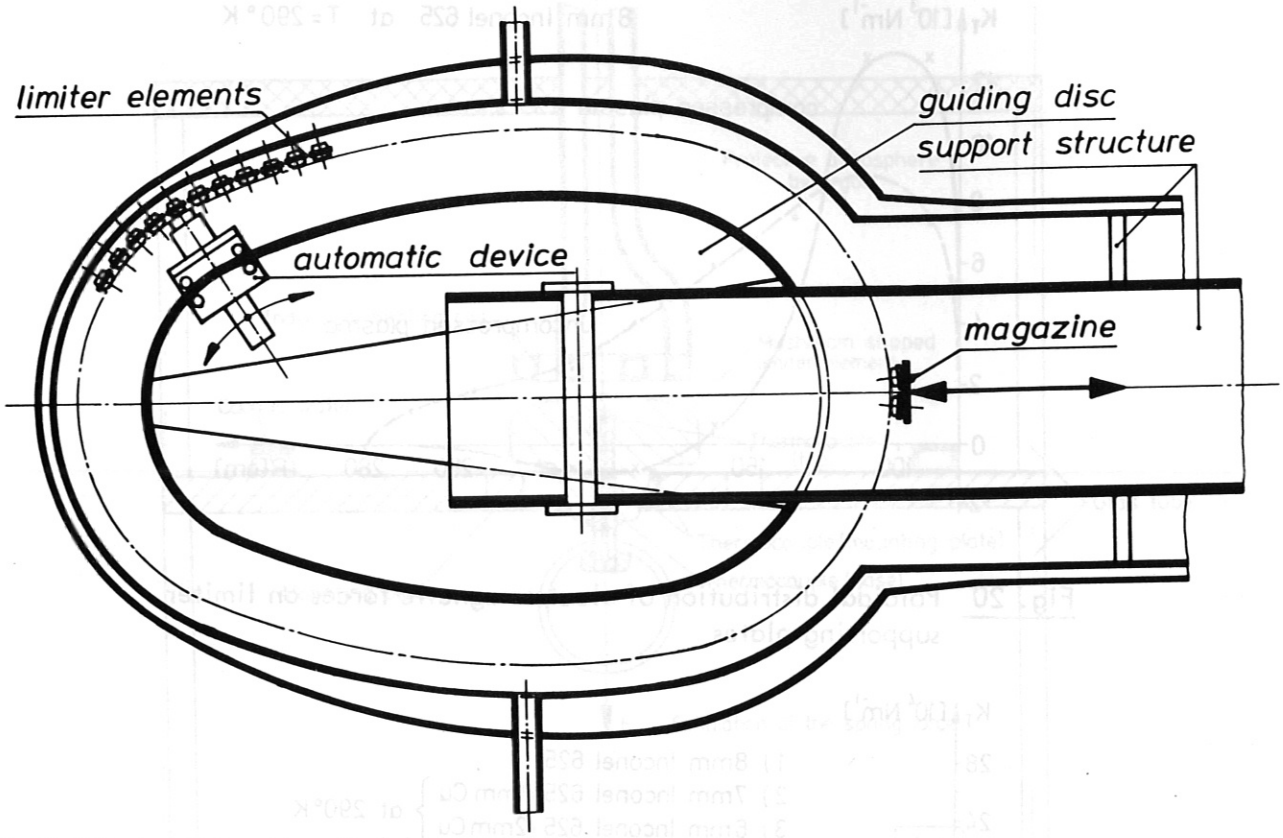

Fig. 23 Mounting and exchange of limiter elements using an automatic device

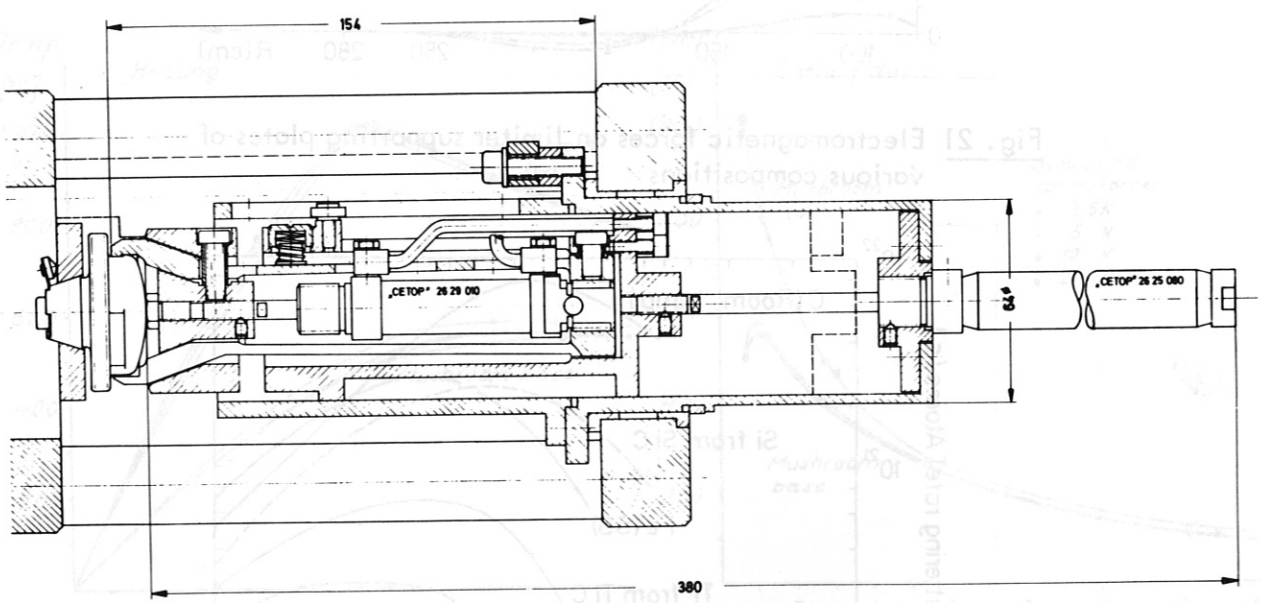

Fig. 24 Prototype of the automatic device for mounting of the limiter elements

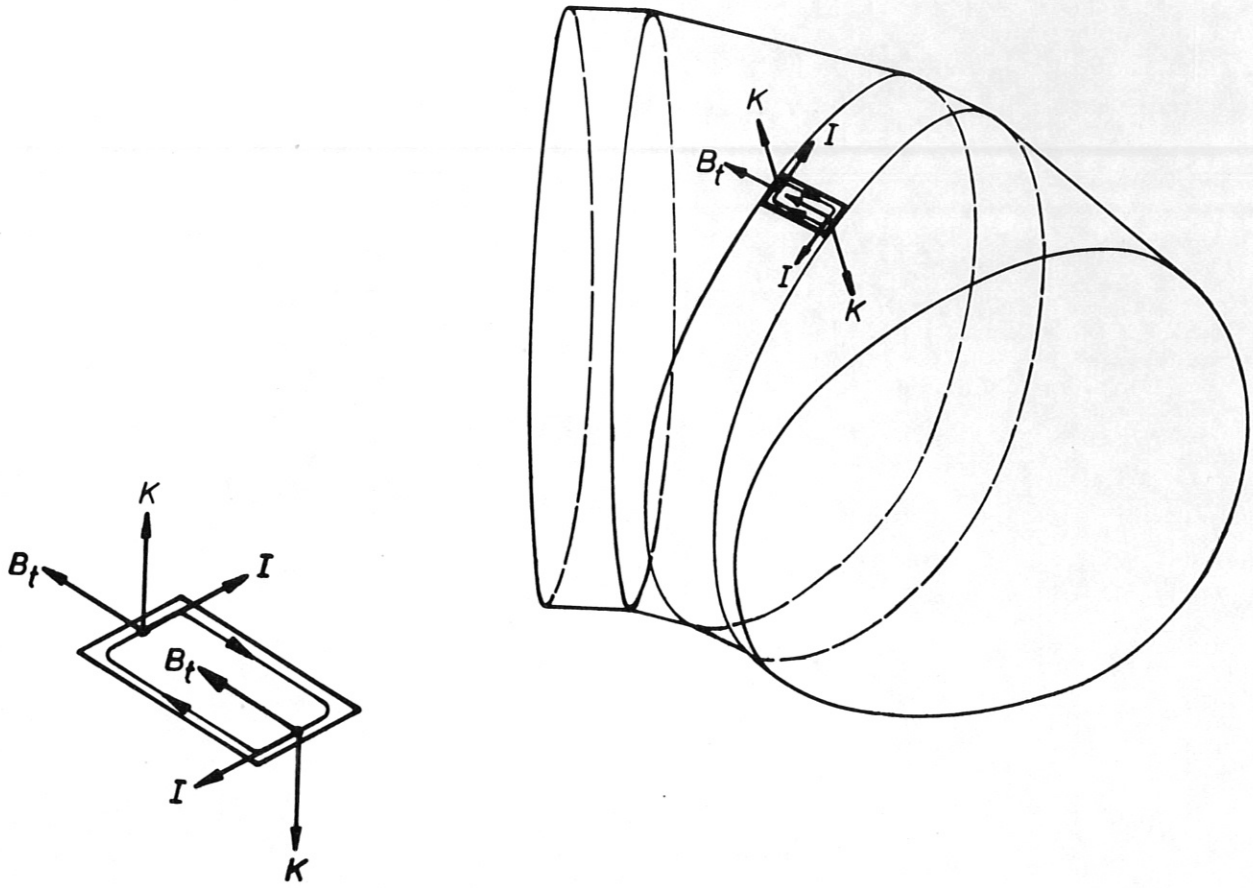

Fig. 25 Direction of tilting forces at the limiter supporting plates in case of a hard plasma disruption